

PUBLIC RELEASE DATE: 4-Jun-2014

[[Print](#) | [E-mail](#)] [+](#) [Share](#) [[Close Window](#)]

Contact: Kate Greene
kgreene@lbl.gov
510-486-4404
[DOE/Lawrence Berkeley National Laboratory](#)

Surprisingly strong magnetic fields challenge black holes' pull

Analysis of radio waves from black holes shows long-neglected magnetic fields have an unexpected presence

A new study of supermassive black holes at the centers of galaxies has found magnetic fields play an impressive role in the systems' dynamics. In fact, in dozens of black holes surveyed, the magnetic field strength matched the force produced by the black holes' powerful gravitational pull, says a team of scientists from the U.S. Department of Energy's Lawrence Berkeley National Laboratory (Berkeley Lab) and Max Planck Institute for Radio Astronomy (MPIfR) in Bonn, Germany. The findings are published in this week's issue of *Nature*.

"This paper for the first time systematically measures the strength of magnetic fields near black holes," says Alexander Tchekhovskoy, the Berkeley Lab researcher who helped interpret the observational data within the context of existing computational models. "This is important because we had no idea, and now we have evidence from not just one, not just two, but from 76 black holes."

Previously, Tchekhovskoy, who is also a postdoctoral fellow at the University of California, Berkeley, had developed computational models of black holes that included magnetic fields. His models suggested a black hole could sustain a magnetic field that was as strong as its gravity, but there was not yet observational evidence to support this prediction. With the two forces balancing out, a cloud of gas caught on top of the magnetic field would be spared the pull of gravity and instead levitate in place.

The magnetic field strength was confirmed by evidence from jets of gas that shoot away from supermassive black holes. Formed by magnetic fields, these jets produce a radio emission. "We realized that the radio emission from black holes' jets can be used to measure the magnetic field strength near the black hole itself," says Mohammad Zamaninasab, the lead author of the study, who did the work while at MPIfR.

Other research teams had previously collected radio-emission data from "radio-loud" galaxies using the Very Long Baseline Array, a vast network of radio telescopes in the United States. The researchers analyzed this pre-existing data to create radio-emission maps at different wavelengths. Shifts in jet features between different maps let them calculate the field strength near the black hole.

Based on the results, the team found not only that the measured magnetic fields can be as strong as a black hole's gravity, but that they are also comparable in strength to those produced inside MRI machines found in hospitals--roughly 10,000 times greater than the field of the Earth itself.

Tchekhovskoy says the new results mean theorists must re-evaluate their understanding of black-

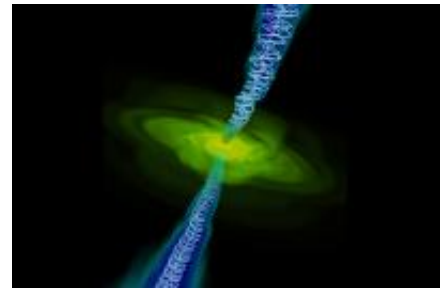


IMAGE: This is a computer simulation of gas (in yellow) falling into a black hole (too small to be seen). Twin jets are also shown with magnetic field lines.

[Click here for more information.](#)

hole behavior. "The magnetic fields are strong enough to dramatically alter how gas falls into black holes and how gas produces outflows that we do observe, much stronger than what has usually been assumed," he says. "We need to go back and look at our models once again."

###

Lawrence Berkeley National Laboratory addresses the world's most urgent scientific challenges by advancing sustainable energy, protecting human health, creating new materials, and revealing the origin and fate of the universe. Founded in 1931, Berkeley Lab's scientific expertise has been recognized with 13 Nobel prizes. The University of California manages Berkeley Lab for the U.S. Department of Energy's Office of Science. For more, visit <http://www.lbl.gov>.

 Back To
EurekAlert! [[Print](#) | [E-mail](#)  [Share](#)] [[Close Window](#)]

AAAS and EurekAlert! are not responsible for the accuracy of news releases posted to EurekAlert! by contributing institutions or for the use of any information through the EurekAlert! system.

[HOME](#) [DISCLAIMER](#) [PRIVACY POLICY](#) [TERMS & CONDITIONS](#) [CONTACT US](#) [TOP](#)

Copyright ©2014 by AAAS, the science society.

Near Term Presentations Involving Ignitor

- Technology Review Symposium (B. Coppi, Bologna, May 5)
- Rome Symposium (G. Valli)
- FESAC Meeting 8 July, Washington, DC)
- Applied Superconductivity Conference (Charlotte, NC, 10-15 August)
- Scripps Inst. (28, 29 August, San Diego)
- IAEA (13-17 October, St. Petersburg)
- SOFT Conference (29 October-3 October, San Sebastian, Spain)
- APS Meeting (27-31 October, New Orleans)

Deadline for the APS Meeting: 11 July 2014

Relevance of the Document of the General Accounting Office (June 2014)

Gentile professore,

la frase sull'ignizione tratta dal PCAST Panel on the U.S. Fusion Energy R&D Program del 1995 con John Holdren come Chair e' la seguente:

Producing an ignited plasma will be a truly notable achievement for mankind and will capture the public's imagination. Resembling a burning star, the ignited plasma will demonstrate a capability with immense potential to improve human well-being. Ignition is analogous to the first airplane flight or the first vacuum-tube computer. As in those cases, the initial model need not resemble the one that is later commercialized; much of what would be learned in a tokamak ignition experiment would be applicable both to more advanced tokamak approaches and to other confinement concepts.

e si trova al fondo di pagina 25.

The New York Times

October 18, 2012

Andrew Revkin

With Tight Research Budgets, Is There Room for the Eternal Promise of Fusion?

I think it's about as clear and balanced an account as could be fit into this amount of space. If I were to add a little bit, I'd note that both magnetic and inertial-confinement fusion studies can stand comparison with most other domains of "big physics" fundamental research, in terms of the pace at which they have generated new knowledge in physics as well as spin-off technologies useful in other domains of science and practice. If somebody wanted a lot more, I'd refer them to the opening chapters of the PCAST review of the US fusion research program that I chaired for President Clinton in 1995, which is at <http://www.whitehouse.gov/sites/default/files/microsites/ostp/pcast-95-f...>

(The later chapters are somewhat dated, of course, but the opening ones outline the rationale for pursuing fusion research and the metrics for evaluating it in a way I'm still happy with.)

JOHN P. HOLDREN, PhD

Assistant to the President for Science and Technology
and Director, Office of Science and Technology Policy
Executive Office of the President of the United States



June 2014

FUSION ENERGY

Actions Needed to Finalize Cost and Schedule Estimates for U.S. Contributions to an International Experimental Reactor

Contents

Letter		1
	Background	6
	The Estimated Cost and Schedule of the U.S. ITER Project Has Grown Substantially Since 2006	15
	Despite Reflecting Most Characteristics of Reliable Cost and Schedule Estimates, DOE's Estimates Cannot Be Used to Set a Baseline in Part Because They Are Linked to an Unreliable International Schedule	21
	DOE Has Taken Actions to Reduce U.S. ITER Project Costs but Has Not Adequately Planned for Their Impact on the U.S. Fusion Program	30
	Conclusions	36
	Recommendations for Executive Action	38
	Agency Comments and Our Evaluation	38
Appendix I	Objectives, Scope, and Methodology	40
Appendix II	List of Experts	45
Appendix III	Status of U.S. Hardware Components for the International Thermonuclear Experimental Reactor (ITER) as of August 2013	46
Appendix IV	GAO Assessment of DOE's Current (August 2013) Cost Estimate for the U.S. International Thermonuclear Experimental Reactor (ITER) Project Compared with Best Practices	48
Appendix V	GAO Assessment of DOE's Current (August 2013) Schedule Estimates for the Two Largest Hardware Items of the U.S. International Thermonuclear Experimental Reactor (ITER) Project Compared with Best Practices	50

Appendix VI	Comments from the Department of Energy	51
Appendix VII	GAO Contact and Staff Acknowledgments	53
Tables		
	Table 1: U.S. Hardware Components to Be Delivered to the ITER Organization	12
	Table 2: Four Characteristics of High-Quality, Reliable Cost and Schedule Estimates	22
Figures		
	Figure 1: The Fusion Reaction	6
	Figure 2: Aerial View of Construction Progress at the ITER Site as of June 2013	9
	Figure 3: Countries Participating in ITER and ITER Site Location	11
	Figure 4: U.S. ITER Project Share of the U.S. Fusion Program Budget, Fiscal Years 2006-2015	13
	Figure 5: Total Estimated Cost and Completion Date for the U.S. ITER Project	16

Abbreviations

DOE	Department of Energy
ITER	International Thermonuclear Experimental Reactor
OMB	Office of Management and Budget
OSTP	Office of Science and Technology Policy
State	Department of State

This is a work of the U.S. government and is not subject to copyright protection in the United States. The published product may be reproduced and distributed in its entirety without further permission from GAO. However, because this work may contain copyrighted images or other material, permission from the copyright holder may be necessary if you wish to reproduce this material separately.

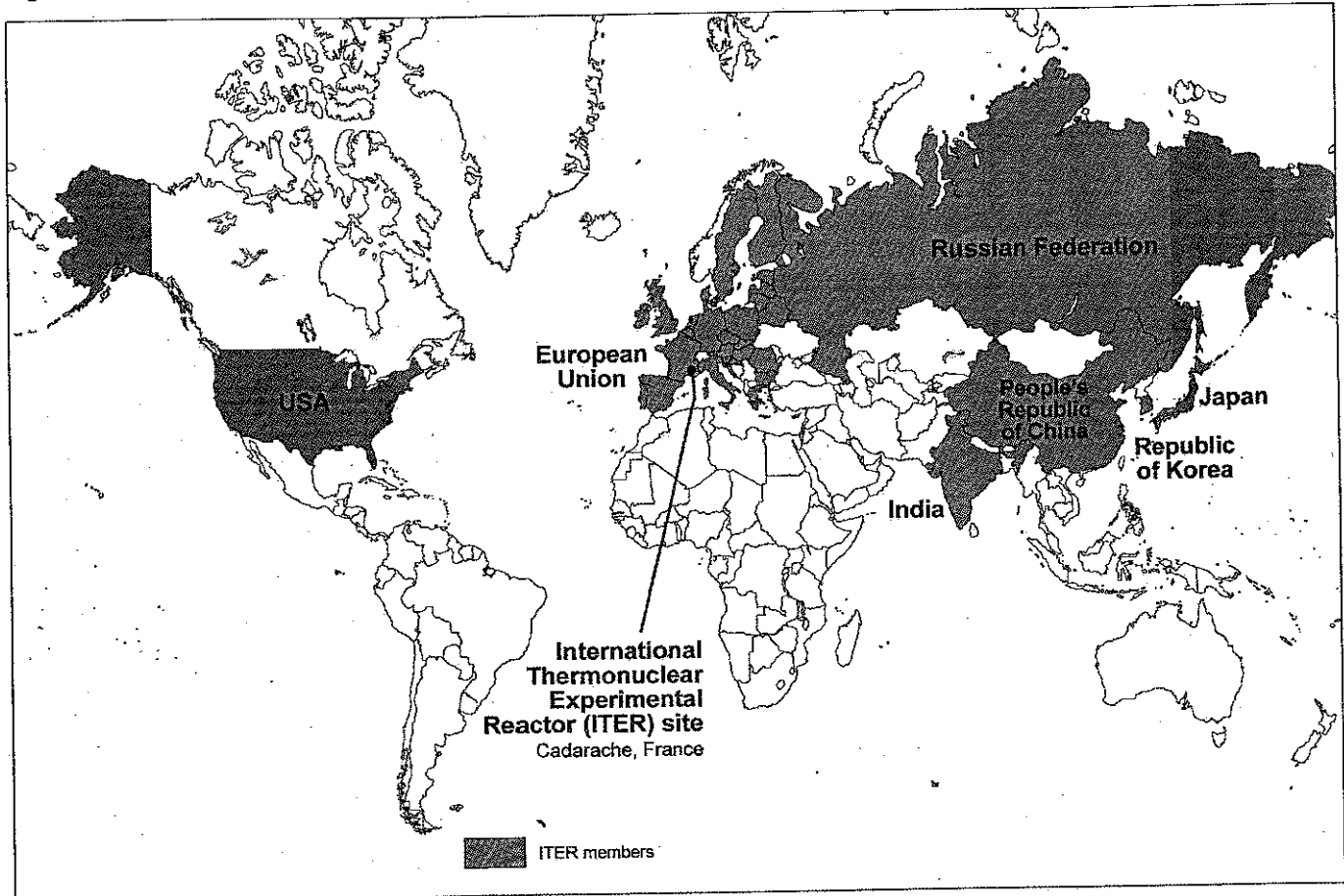
generating more power than it consumes. Magnetic fusion uses magnetic devices to confine a plasma, consisting of electrically charged atoms, and sustain a fusion reaction.¹² ITER will be a magnetic fusion device known as a "tokamak."¹³ To reduce the risk of investing in only one device, DOE's Office of Fusion Energy Sciences also funds scientific research on alternative types of magnetic devices. Inertial fusion relies on intense lasers or particle beams to heat and compress a small, frozen pellet of deuterium and tritium—a few millimeters in size—that would yield a burst of energy. The lasers or particle beams would continuously heat and compress the pellets, which would simulate, on a very small scale, the actions of a hydrogen bomb. The National Nuclear Security Administration, a separately organized agency within DOE, is leading efforts in inertial fusion because it can be used for defense needs, such as validating the integrity and reliability of the U.S. nuclear weapons stockpile.

ITER is considered to be the next step in magnetic fusion. It is an experiment to study fusion reactions in conditions similar to those expected in a future electricity-generating power plant. The goal is to be the first fusion device in the world to produce a substantial amount of net power—that is, produce more power than it consumes. Specifically, the objective is to produce 10 times more power than is needed to start the fusion reaction in pulses of 5 or more minutes. ITER also will test a number of key technologies, including the heating, control, and remote maintenance systems that will be needed for a fusion power station. ITER has been planned to consist of four phases: (1) construction, (2) operation, (3) deactivation, and (4) decommissioning. The construction phase, which is the sole focus of the U.S. ITER Project, began in 2007 (see fig.2 for an aerial view of construction progress at the ITER site as of June 2013). The international project schedule, as of April 2014, anticipates that the ITER fusion device will be built by 2019 and achieve

¹²Current magnetic devices have not been able to sustain this fusion reaction for more than a few seconds, not the long period of time that the reaction would need to be sustained to produce electricity.

¹³The term "tokamak" comes from a Russian acronym for a fusion device that was developed in the former Soviet Union during the 1950s and 1960s. A tokamak has been the most successful magnetic fusion device, but there is still uncertainty that it will lead to a commercially viable fusion energy device.

Figure 3: Countries Participating in ITER and ITER Site Location



Sources: GAO; Map Resources (map). | GAO-14-499

Under the ITER Agreement, the United States is responsible for 9.09 percent of ITER's total construction cost.¹⁵ DOE fulfills this obligation by supplying personnel to work for the ITER Organization; by making cash contributions to the ITER Organization to cover common expenses; and

¹⁵The United States will also be responsible in the future for 13 percent of the costs of operating, deactivating, and decommissioning ITER. These costs—which DOE estimated would be about \$1.5 billion when the ITER Agreement was signed in 2006—are not included in U.S. ITER Project cost estimates because the U.S. ITER Project only covers U.S. contributions to ITER's construction phase.

requirements, uncertainty about the ITER Organization's performance, and the dependence on other ITER members for production of items that are used in U.S. hardware components. To better account for these risks and uncertainties, the review added additional amounts to DOE's current cost estimate of \$3.915 billion and found that the U.S. ITER Project was more likely to cost from \$4 billion to \$6.5 billion.⁴² The reviewers recommended, among other things, that the U.S. ITER Project Office update its risk estimates to be more comprehensive and reevaluate its risk mitigation assessments before DOE approves a performance baseline for the U.S. ITER Project.

In the absence of a performance baseline, DOE has developed a 2-year plan for the U.S. ITER Project that sets near-term cost and schedule targets to guide the project's performance in fiscal years 2013 and 2014.⁴³ However, this 2-year plan is an interim measure and does not represent DOE's commitment to a specific cost and schedule for the U.S. ITER Project as a performance baseline would. Most of the fusion energy and project management experts we interviewed emphasized the importance of DOE approving a performance baseline for the U.S. ITER Project, with some experts noting that a performance baseline would provide a goal for all project stakeholders to work toward and might ease concerns about the uncertainty of the funding levels needed to complete the project. Several experts also told us that, until DOE approves a performance baseline for the U.S. ITER Project, there will continue to be uncertainty about the project's direction.

⁴²DOE, in its fiscal year 2015 budget request, identified the internal peer review's suggested cost range of \$4 billion to \$6.5 billion as the best estimate for the U.S. ITER Project's potential cost. According to DOE officials, the internal peer review's cost range was not a detailed cost estimate like the U.S. ITER Project Office's \$3.915 billion estimate. Rather, the range reflected amounts added to the \$3.915 billion estimate by peer review officials to address their assessment that the U.S. ITER Project Office estimate did not sufficiently consider all project risks and uncertainties. Four of the 10 fusion energy and project management experts we interviewed said they thought the internal peer review's cost range was overstated and unrealistic, with 2 of the experts stating that the review committee used a worst case scenario, which they do not view as likely, to develop the higher end of the cost range.

⁴³DOE officials told us that the interim 2-year plan also allows the agency to formally monitor project progress.

In attesa della riforma della dirigenza pubblica (per ora rinviata al 2015), il presidente del Consiglio prosegue con la sua personale rivoluzione dal basso. Ha nominato - ed è la prima volta - una donna, Rossella Orlandi, all'Agenzia dell'Entrate. Ha poi finalmente integrato la Consob (la commissione che vigila sui mercati finanziari) con la docente di diritto commerciale Anna Genovese. E a rappresentare l'Italia alla Nato ha mandato un'altra donna, Mariangela Zappia, diplomatica che già rappresentava la Ue all'Onu.

Nei primi cento giorni di governo la rottamazione del premier ha finalmente cominciato ad incidere anche sulla burocrazia. Ha iniziato usando la legge dello spoils system per cambiare tre quarti dei capi gabinetto. Sebbene nella maggior parte dei casi si sia limitato a spostarli da un ministero all'altro, comunque li ha spostati, con una tecnica che prima di lui aveva seguito solo il governo di Carlo Azeglio Ciampi.

Poi è venuto il turno dei capi dipartimento della Presidenza del consiglio. Come si legge nella nuova pagina web di palazzo Chigi - che ora pubblica informazioni finora monopolio degli iniziati dei meandri romani - alla presidenza del consiglio sono cambiate quasi tutte le persone che occupano le posizioni più rilevanti. Nei quattro dipartimenti di indirizzo generale (affari giuridici e legislativi, coordinamento amministrativo, editoria ed informazione, risorse umane) sono arrivati quattro nuovi capi. Nei tanti (dodici) dipartimenti con funzioni specifiche i nuovi capi sono nove, più due incaricati ad interim, per un totale di undici novità. Come nel caso dei nuovi capi gabinetto, i neo-nominati hanno una caratteristica comune. Sono tutti giuristi, tranne due: Antonio Naddeo, laureato in economia e Giovanni Serpelloni, medico chirurgo con un master in general management. Nell'insieme, per sfuggire alla ragnatela dei mandarini (i dirigenti pubblici sostanzialmente inamovibili che hanno il potere di ritardare sine die i decreti attuativi senza i quali le leggi sono documenti vuoti), Renzi si è dotato di un gruppo di nuovi dirigenti, prevalentemente cinquantenni e quarantenni - quindi giovani per gli standard italiani, dato che nel 2012 il dirigente ministeriale medio aveva 52 anni - e per metà donne (erano un terzo nel 2012).

Forse qualche dirigente con una formazione scientifica avrebbe portato un pò di aria nuova, e soprattutto un diverso modo di affrontare i problemi. Per vedere un ingegnere chiamato a gestire qualcuna delle tante procedure di Palazzo Chigi bisogna attendere ancora.

E' anche un peccato che Renzi non abbia approfittato di questa piccola rivoluzione per creare una figura, il consigliere del primo ministro per la scienza e la tecnologia, che è presente e svolge un ruolo importante

nella maggior parte dei paesi - ad esempio è una delle posizioni più senior nella Casa Bianca. Renzi potrebbe chiedergli un parere indipendente su Iter, un progetto che si propone di realizzare un reattore sperimentale a fusione nucleare, al quale l'Italia partecipa con sette altri paesi (Ue, Stati Uniti, Cina, India, Giappone, Russia e Corea). Iter sta investendo 13 miliardi di euro - quasi triplicati dalla stima iniziale del 2001 – mentre la comunità scientifica, diversamente dai burocrati ministeriali (vedi *Science* 18 aprile 2014, p.243), ritiene sia un progetto che non va da nessuna parte.

Francesco Daveri e Francesco Giavazzi

More Basic Research at the National Ignition Facility

By Michael Lucibella

APS News June 2014 (Volume 23, Number 6)

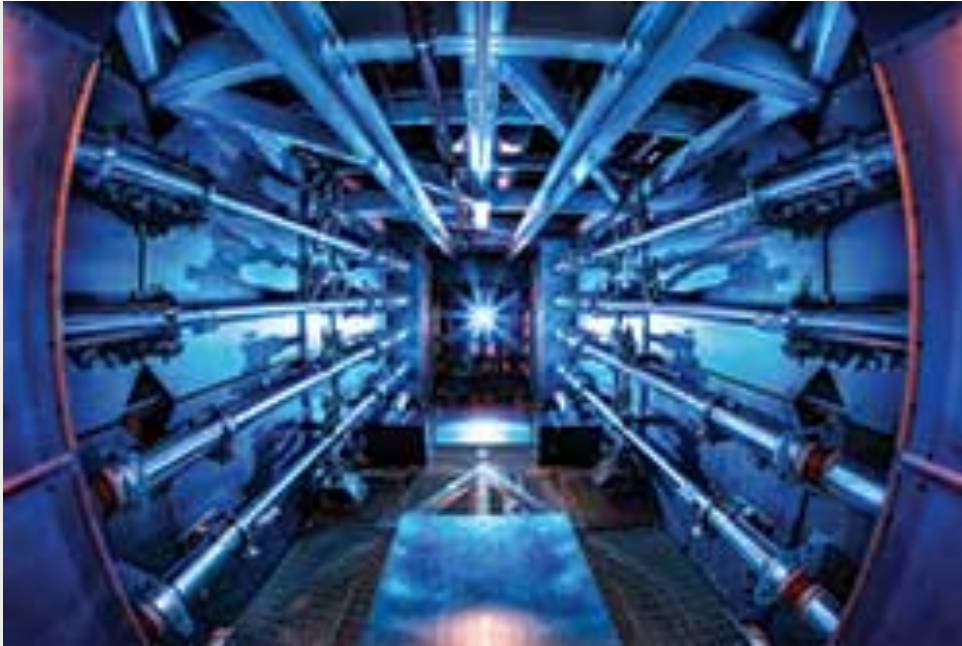


Photo courtesy of Lawrence Livermore National Laboratory

Brighter days ahead — outside researchers will get more time at one of the largest laser facilities in the world.

Recent changes at the nation's top large laser facility are making it easier for scientists to do basic research there. Though still primarily focused on fusion and nuclear weapons research, the National Ignition Facility (NIF) at Lawrence Livermore National Laboratory is becoming more of a user facility.

“There's been a real sea change at NIF for the better in terms of the fundamental science program,” said Don Lamb, chair of the NIF users group. “It's a transformation of what NIF can do for the scientific community.”

Completed in 2009, NIF's primary missions are to simulate nuclear weapon detonations as part of the Department of Energy's (DOE) “Stockpile Stewardship” program and to develop laser fusion to generate electricity. NIF concentrates 192 powerful lasers onto a 0.5 cm diameter pellet of hydrogen, compressing it and igniting nuclear fusion reactions. The energy program's ultimate goal is to get more energy output from the process than input.

“Ignition is only part of what NIF was built for and what it is actually doing,” said Jon Eggert, a researcher at Livermore. “There’s actually a fairly large contingent of people that want to do fundamental science on NIF.”

While its dual primary missions take up about 90 percent of the facility’s laser blasts, or “shots,” the thin slot for other fundamental science is enlarging. New scheduling policies will give independent researchers more time and shots on the machine.

“The real issue has been that for many years there were virtually no shots allocated to the fundamental science program,” Lamb said. “This went along with an incredible single-minded focus pursuing ignition through a single path.”

Before the facility was completed, the DOE put out a call for proposals to do fundamental science at the facility. A number of researchers responded, and the NIF offices assigned nine teams their own shots at the laser facility.

Parceling out a set number of shots, however, rather than blocks of time as at other user facilities, brought about backups and delays at the lab. Experiments that weren’t ready by their scheduled shot day would keep tying up the machine until they were ready, delaying other experiments. This slipping schedule made it difficult for scientists and graduate students to plan their trips to Livermore in advance.

In addition, there weren’t many fundamental science shots to start with. In 2009 there were two shots allotted to fundamental science. The next year there was one. The numbers slowly started to increase. There were four fundamental science shots in both 2011 and 2012 and seven in 2013. This year is slated to have eight shots. Researchers originally hoped for more, but budget cuts from the US government’s funding sequestration cut the total number of shots for all experiments.

“We just haven’t had enough shots to [accommodate] all of those teams,” said Chris Keane, the director of the NIF user office at Livermore. “We are looking at issuing a new call soon.”

For the new lineup of experiments, the NIF leadership is revamping the scheduling system. Research teams will be able to apply for a set number of days

at the NIF and can shoot the lasers as much or as little as they need to during that time.

“Because it’s shot days, if you’re not ready, they won’t wait for you,” Lamb said. “That’s going to help not only the NIF be efficient.... It’s also going to help, I think, the academic experimental groups.”

The lab is also working to increase the total number of shots for all types of science. In 2013 there were a total of 209 laser shots. Because of sequestration, the number for 2014 is down to about 150, but lab administrators are hoping to have between 250 and 300 shots in 2015, and about 300 in 2016. Right now administrators are scheduling experiments for the spring of 2015.

The changes came about in part from a recent study mandated by the Senate Appropriations Committee to find ways to increase the number of shots and overall science output at the machine.

In addition, recent leadership changes at Livermore put people in positions to build up the fundamental science at the NIF. The lab’s new director, William Goldstein, has been widely credited for advocating for fundamental science at NIF since its inception. Similarly, Jeff Atherton was named head of NIF in May of 2013 and is also seen as a strong proponent of basic research.

“Jeff is very transparent and open about issues we have to overcome,” Lamb said. “He’s doing everything he can to increase the science being done at the NIF.”

There are other laser facilities across the country that can do similar experiments at lower energy. The Jupiter Laser Facility at Livermore and the Omega Laser at the University of Rochester are essentially older, smaller versions of the NIF that do laser compression science.

“[NIF] is just a totally new regime,” Keane said. “It’s the energy, but it’s also the precision and the reproducibility.” Experiments at NIF have probed the phases of hydrogen at high densities, how stars form in the Eagle Nebula, and how hydrodynamic instabilities affect supernovas. There have also been about 60 “ride-along” shots that take data during a dedicated fusion energy or stockpile stewardship shot (mostly nuclear cross-section experiments).

Jon Eggert uses the lasers at the NIF to explore the properties of matter at the center of gas giant planets. Astronomers have discovered hundreds of confirmed

exoplanets, but no one knows what molecular and material structures are at the core of the largest planets.

“If we want to answer those sorts of questions, we actually have to know what’s happening on the inside of those planets,” Eggert said. “To do that we need to have experiments.”

Tridimensional Igniting Structures in Fusion Burning Plasmas*

B. Coppi

MIT

Presented at the Ignitor Physics Meeting, Rome, April 3, 2014 and at the Sherwood Theory Meeting, San Diego, CA, March 24, 2014. *Sponsored in part by the U.S. Department of Energy.

Tridimensional Toroidal Modes

Represented by electron temperature (linearized) perturbations of the form

$$\hat{T}_e = \tilde{T}_e (r - r_0) \exp(\gamma t + im^0 \theta - in^0 \zeta)$$

where

$$m^0 \frac{B_\theta}{r_0}(r_0) - n^0 \frac{B_\zeta}{R_0} = 0.$$

Therefore

$$\frac{\mathbf{B}}{B} \cdot \nabla \hat{T}_e \simeq \frac{i}{B} \frac{m^0}{r_0} \frac{dB_\theta}{dr} (r - r_0) \hat{T}_e \equiv i \frac{m^0}{r_0} \frac{r - r_0}{L_s} \hat{T}_e$$

and, for $q(r) \simeq B_\zeta r / (B_\theta R_0)$,

$$\hat{T}_e \simeq \tilde{T}_e (r - r_0) \exp \left\{ \gamma t + in^0 [q(r_0)\theta - \zeta] \right\},$$

considering that the modes which will be identified are localized over a distance $\delta_r \ll r_0$.

Clearly these are not ballooning modes but can be viewed as “quasi-flute” modes.

We assume that in the initial state the electron and nuclei temperatures are equal. The simplified total thermal energy balance equation for the electron and the nuclei population that we consider, referring to the relevant linearized form of the perturbations, is

$$\frac{3}{2}n\frac{\partial}{\partial r}(\hat{T}_e + \hat{T}_i) \approx \alpha_F n^2 T_i \hat{T}_i - \alpha_B n^2 \frac{\hat{T}_e}{T_e^{1/2}} + n \frac{\partial}{\partial l} D_{\parallel}^e \frac{\partial}{\partial l} \hat{T}_e + n \frac{\partial}{\partial r} D_{\perp}^e n \frac{\partial \hat{T}_e}{\partial r} .$$

As this equation shows, the electron thermal energy transport is assumed to be prevalent. Moreover, α_F and α_B are about constant in the range of temperatures of interest, $\alpha_F n^2 T_i^2$ indicating the rate of electron thermal energy gained from the slowing down of the ${}^4\text{He}$ nuclei produced by D-T fusion reactions and $\alpha_B n^2 T_e^{1/2}$ indicating the range of energy loss by bremsstrahlung radiation emission. The electron thermal energy transport transverse and longitudinal to the magnetic field is included by the diffusion coefficients D_{\perp}^e and D_{\parallel}^e ,

respectively. In the following we shall neglect the contribution of $\alpha_B n^2 T_e^{1/2}$ as we consider temperatures well above the relevant ideal ignition temperature.

If, for the sake of simplicity we consider a radial profile

$$\tilde{T}_e(r - r_0) \simeq \tilde{T}_e^0 \exp\left(-\sigma (r - r_0)^2 / 2\right)$$

we obtain

$$\hat{T}_e \left(\frac{3}{2} \gamma + v_T + k_{\parallel}^2 D_{\parallel}^e + \sigma D_{\perp}^e - (r - r_0)^2 D_{\perp}^e \sigma^2 \right) = (v_T + \alpha_F n T_i) \hat{T}_i$$

where

$$k_{\parallel} \simeq \frac{n^0}{qR_0} \frac{dq}{dr} (r - r_0)$$

and

$$\sigma^2 = \frac{D_{\parallel}^e}{D_{\perp}^e} \left(\frac{n^0}{qR_0} \right)^2 \left(\frac{dq}{dr} \right)^2.$$

A form of the thermal energy balance equation of the nuclei that is compatible with the radial profile

$$\tilde{T}_i = \tilde{T}_i^0 \exp(-\sigma x^2/2),$$

where $x \equiv r - r_0$, is

$$\frac{3}{2} n \frac{\partial \hat{T}_i}{\partial t} \simeq 3 \frac{m_e}{m_i} v_{ei} (\hat{T}_e - \hat{T}_i) n - k_{\parallel}^2 D_{\parallel}^i \hat{T}_i n + D_{\perp}^i \frac{\partial^2 \hat{T}_i}{\partial x^2} n - \Delta v_D^i n \hat{T}_i$$

where $\Delta v_D^i n T$ represents the thermal energy loss rate that is not represented by D_{\parallel}^i and D_{\perp}^i with the ratio

$$\frac{D_{\parallel}^i}{D_{\perp}^i} = \frac{D_{\parallel}^e}{D_{\perp}^e}$$

Then

$$\hat{T}_i \simeq \frac{v_T}{\frac{3}{2}\gamma + v_T + v_D^i} \hat{T}_e.$$

where $v_D^i = \Delta v_D^i + \sigma D^i$ and

$$v_T \equiv 3 \frac{m_e}{m_i} v_{ei}$$

The relevant dispersion relation is

$$\frac{9}{4}\gamma^2 + \frac{3}{2}\gamma(v_D^i + v_D^i + 2v_T) \approx \gamma_F v_T - \left[v_D^i v_D^2 + v_T (v_D^i + v_D^e) \right].$$

where $\gamma_F \equiv 2\alpha_F n T_i$, and

$$v_D^e = \sigma D_{\perp}^e = \left(D_{\perp}^e D_{\parallel}^e \right)^{1/2} \left| \frac{k_y}{L_s} \right|.$$

It is evident that the instability condition is

$$\gamma_F > \frac{v_D^i v_D^e}{v_T} + (v_D^i + v_D^e)$$

and represents a well defined local ignition condition. We note that

$$\frac{v_D^i v_D^e}{v_T} \sim \frac{m_i}{3v_{ei}m_e} v_D^i \left(\frac{n^0}{qR_0} \frac{dq}{dr} \right) (D_{\parallel}^e D_{\perp}^e)^{1/2}$$

and that $\gamma_F > v_D^i v_D^e / v_T$ can be viewed as favoring “low temperature” ignition, given that $\gamma_F \propto nT_i$.

References

B. Coppi, M.N. Rosenbluth and R. Z. Sagdeev, *Phys. Fluids* **10**, 582 (1967).

S.I. Braginski, “Transport Processes in a plasma”, *Reviews of Plasma Physics* Vol. 1 (Consultants Bureau, New York, 1965), P. 205.

Simplest Asymptotic Limit of Complex Reconnecting Modes

$$\mathbf{B} \simeq \mathbf{B}_0 \mathbf{e}_z + B_y(x) \mathbf{e}_y$$

$$\hat{B}_x = \tilde{B}_x(x) \exp(i\omega t + ik_y y + ik_z z)$$

$$\hat{v}_x \simeq -i\omega \hat{\xi}_x$$

$$\mathbf{k} \cdot \mathbf{B} \simeq k_y B'_y(x - x_0)$$

Inner Region (electron momentum conservation component)

$$-i(\omega - \omega_{*T})\tilde{B}_{x0} \approx i(k_y B_y')(x - x_0)\tilde{\xi}_x[-i(\omega - \omega_*)] + D_m \frac{d^2 \tilde{B}_x}{dx^2} \quad (1)$$

$$\omega_* \equiv -k_y D_B \frac{1}{n} \frac{dn}{dx} \quad D_B \equiv \frac{cT_e}{eB}$$

$$\omega_{*T} + \omega_* \left[1 + (1 + \alpha_T) \frac{d \ln T_e / dx}{d \ln n / dx} \right]$$

$$D_m = \frac{\eta c^2}{4\pi} \quad \tilde{B}_x \approx \tilde{B}_{x0}$$

Outer Region

$$\tilde{B}_x \approx (\mathbf{k} \cdot \mathbf{B}) \tilde{\xi}_x \quad (2)$$

Problems with $\omega - \omega_*$ $\omega - \omega_{*T}$

$$\frac{d^2 \tilde{B}_x}{dx^2} \left(k^2 + \frac{\mathbf{k} \cdot \mathbf{B}''}{\mathbf{k} \cdot \mathbf{B}} \right) \tilde{B}_x \approx 0 \quad (3)$$

from the nuclei momentum conservation equation

Connection condition

$$\frac{1}{r_J} = \int_{\delta} \frac{d^2 \tilde{B}_x}{dx^2} \frac{dx}{\tilde{B}_{x0}}$$

$$\frac{1}{r_J} = \frac{1}{\tilde{B}_{x0}} \left[\frac{d\tilde{B}_x}{dx} \Big|_{x \rightarrow x_0+0} - \frac{d\tilde{B}_x}{dx} \Big|_{x \rightarrow x_0+0} \right]$$

$$\mathbf{k} \cdot \mathbf{B}'' \propto k_y \frac{dJ_{\parallel}}{dx}$$

$$J_{\parallel} = \frac{1}{B} \mathbf{J} \cdot \mathbf{B} \simeq J_z$$

Best variables

$$Z_* \equiv -\frac{\xi_x}{\tilde{B}_{x0}} B'_y k_y \delta$$

$$\bar{x} \equiv \frac{x - x_0}{\delta}$$

δ = characteristic width of the reconnection layer.

$$\tilde{B}_x \simeq \tilde{B}_{x0} \left[1 + \frac{\delta}{r_J} \phi(\bar{x}) \right]$$

$$\frac{\tilde{B}_x''}{\tilde{B}_{x0}} \simeq \frac{1}{D_m} [(\Delta\omega) Z_* \bar{x} + i(\Delta\omega_T)]$$

$$\Delta\omega \equiv \omega - \omega_*$$

$$\Delta\omega_T \equiv \omega - \omega_{*T}$$

Component of the nuclei momentum conservation equation

$$\text{for } \left| \omega \frac{d^2 \tilde{\xi}_x}{dx} \right| \ll D_\mu \left| \frac{d^4 \tilde{\xi}_x}{dx^4} \right|$$

$D_\mu =$ “viscous” diffusion coefficient (should an “inflow” term be included?)

$$\delta \equiv \frac{(D_m D_\mu)^{1/6}}{(k_y \omega_H)^{1/3}}$$

$$\omega_H^2 = \frac{(B'_y)^2}{4\pi n m_i}$$

Then

$$i(\omega - \omega_{di}) \frac{d^4 Z_*}{dx^4} + i(\Delta\omega) \bar{x}^2 Z_* \approx -(\Delta\omega_T) \bar{x}$$

is the equation to be solved

$$\omega_{di} \equiv k_y \frac{c}{eB} \frac{1}{n} \frac{dp_i}{dx}$$

Matching condition

$$\frac{1}{r_j} \approx -\frac{\omega - \omega_{di}}{\delta^5 (k_y \omega_H)^2} D_\mu \int_{-\infty}^{+\infty} \frac{d\bar{x}}{\bar{x}} \frac{d^4 Z}{d\bar{x}^4}$$

$$r_j |\omega - \omega_{di}| \frac{D_\mu}{\delta^5 (k_y \omega_H)^2} = \frac{D_\mu^{1/6} r_j}{D_\mu^{5/6} |k_y \omega_H|^{1/3}} |\omega - \omega_{di}| \sim 1 \quad \text{required.}$$

In addition $\delta \geq \delta_i$ is also required

$$\rho_i = \frac{v_{thi}}{\Omega_{ci}} = \text{ion gyro radius.}$$

If

$$\delta \sim \frac{D_m}{|\omega_{di}|} \geq \rho_i$$

D_m has to be of the order of the Gyro-Bohm diffusion coefficient [*].

$$D_{GB} \sim D_m \frac{\rho_i}{r_{pi}}$$

$$\frac{1}{r_{pi}} \equiv -\frac{1}{\rho_i} \frac{d\rho_i}{dx}$$

If $\omega = \omega_R$ $Z_* = iZ_I$

Therefore the matching condition is impossible.

If $\omega = i\gamma$ $\gamma \gg \omega_R$

$Z_* = iZ_I$

the matching condition is possible. In particular

$$\begin{aligned} \frac{1}{r_j} V_m &= \gamma \int \frac{d\bar{x}}{\bar{x}} Z_I^{IV} - (\omega_R - \omega_{di}) \int \frac{d\bar{x}}{\bar{x}} Z_R^{IV} \\ 0 &= \gamma \int \frac{d\bar{x}}{\bar{x}} Z_R^{IV} + (\omega_R - \omega_{di}) \int \frac{d\bar{x}}{\bar{x}} Z_I^{IV} \end{aligned}$$

$$\frac{1}{r_J} = V_m \left[\gamma + \frac{(\omega_R - \omega_{di})^2}{\gamma} \right] \int \frac{d\bar{x}}{\bar{x}} Z_I^{IV}$$

Note that

$$\gamma \{ Z_I^{IV} + \bar{x}^2 Z_I - \bar{x} \} = (\Delta\omega) \bar{x}^2 Z_e + (\omega_R - \omega_{di}) Z_R^{IV}$$

$$\gamma \{ Z_R^{IV} + \bar{x}^2 Z_R \} \simeq \{ (\Delta\omega_T)_R \bar{x}^2 - (\omega_R - \omega_{di}) Z_I^{IV} - (\Delta\omega)_R Z_I x^2 \}$$

The problem associated with the fact that $(\Delta\omega_T)_R \neq (\Delta\omega)_R$ in dealing with the asymptotic solutions for $\bar{x}^2 \gg 1$ can be resolved by considering an intermediate-outer region.

[*] Coppi, Rosenbluth, Sagdeev, *Phys. Fluids* (1966).

Dynamically important magnetic fields near accreting supermassive black holes

M. Zamaninasab¹, E. Clausen-Brown¹, T. Savolainen¹ & A. Tchekhovskoy^{2,3}

Accreting supermassive black holes at the centres of active galaxies often produce ‘jets’—collimated bipolar outflows of relativistic particles¹. Magnetic fields probably play a critical role in jet formation^{2,3} and in accretion disk physics⁴. A dynamically important magnetic field was recently found near the Galactic Centre black hole⁵. If this is common and if the field continues to near the black hole event horizon, disk structures will be affected, invalidating assumptions made in standard models^{3,6,7}. Here we report that jet magnetic field and accretion disk luminosity are tightly correlated over seven orders of magnitude for a sample of 76 radio-loud active galaxies. We conclude that the jet-launching regions of these radio-loud galaxies are threaded by dynamically important fields, which will affect the disk properties. These fields obstruct gas infall, compress the accretion disk vertically, slow down the disk rotation by carrying away its angular momentum in an outflow³ and determine the directionality of jets⁸.

General relativistic magnetohydrodynamic simulations find that if the accretion disk is threaded with enough poloidal magnetic flux, the flux will be transported inwards and accumulate in the central region of the disk until the ram pressure of the accreting gas is balanced by the magnetic pressure^{3,7}. (Poloidal refers to a vector pointing along the radial and axial directions in a cylindrical coordinate system, with the axial direction aligned with the disk angular momentum axis.) The poloidal flux threading the black hole, Φ_{BH} , then naturally reaches a saturation or equilibrium value of $\sim 50 \left(\dot{M} r_g^2 c \right)^{1/2}$, where \dot{M} is the mass accretion rate, $r_g = GM/c^2$ the black hole gravitational radius, G the gravitational constant, M the black hole mass, and c the speed of light. The magnetic field then dominates the plasma dynamics of the inner disk and modifies the disk structure such that it becomes a ‘magnetically arrested disk’^{3,6,7}. Simulations of magnetically arrested disks also find that if the black hole’s

dimensionless spin parameter is $a_* \gtrsim 0.5$ ($a_* = 0$ refers to a non-rotating black hole and $a_* = 1$ a maximally spinning black hole), then highly relativistic bipolar jets powered by the black hole’s rotational energy via the Blandford–Znajek effect² are ejected^{9,10} with a total power of $\sim \dot{M} c^2$. Among active galactic nuclei (AGN), only about 10% contain powerful radio-emitting jets (that is, are radio-loud AGN)¹¹.

Although we cannot directly measure Φ_{BH} , we can observationally infer the poloidal magnetic flux threading parsec-scale jets, Φ_{jet} , which by the flux freezing approximation is the same as Φ_{BH} for jets produced via the Blandford–Znajek effect (Fig. 1). This inference can be performed via high-angular-resolution radio observations of the so-called core-shift effect¹² (see Methods), which gives a measure of the jet’s co-moving azimuthal magnetic field, $B'_\phi = B_\phi / \Gamma$ (where primes refer to jet co-moving frame quantities, and Γ is jet bulk Lorentz factor). According to standard Blandford–Znajek jet theory, $B_\phi / B_p \propto a_* R_j / r_H$, where R_j is jet cylindrical radius, B_p is the poloidal magnetic field and $r_H = r_g \left(1 + (1 - a_*^2)^{1/2} \right)$ is the black hole event horizon radius. Therefore, $\Phi_{\text{jet}} \approx R_j^2 B_p \propto M R_j B_\phi$, and a more detailed derivation at one parsec downstream of the black hole yields:

$$\Phi_{\text{jet}} = 1.2 \times 10^{34} f(a_*) \Gamma \theta_j \left[\frac{M}{10^9 M_\odot} \right] \left[\frac{B'_{1\text{pc}}}{1 \text{ G}} \right] \quad (1)$$

Here $f(a_*) = a_*^{-1} r_H / r_g$, $B'_{1\text{pc}}$ is the jet’s co-moving frame magnetic field measured by the core-shift effect, θ_j is the jet opening angle and Φ_{jet} is in units of G cm^2 (for a full derivation of equation (1), see Methods).

The amount of magnetic flux predicted to thread a black hole in the magnetically arrested disk model can be calculated for a given source if its mass and accretion disk luminosity are known. This predicted flux

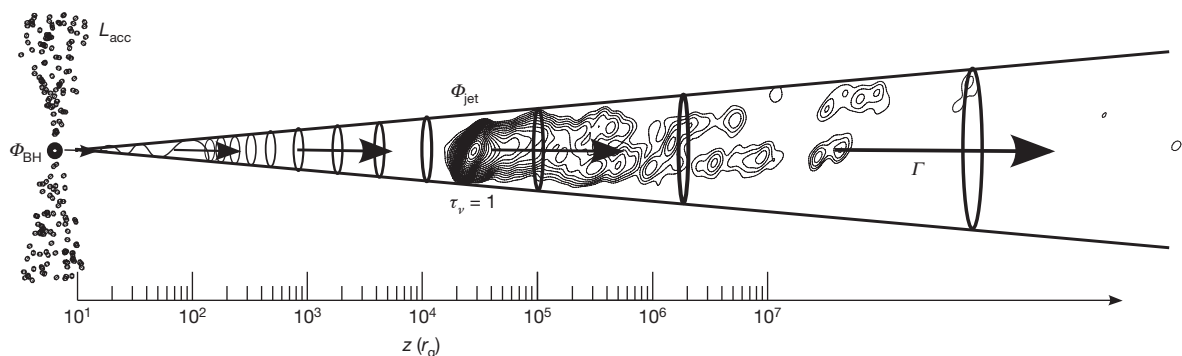


Figure 1 | Diagram of an AGN jet. At left, the large black dot represents the black hole, with the disk (seen side-on) extending up and down; z (horizontal axis) represents the distance above the disk, in units of r_g . The radio core is the bright feature at the upstream end of the parsec-scale jet in the embedded radio image and it corresponds to the place in the jet where the optical depth $\tau_\nu = 1$ for an observing frequency, ν . The frequency-dependent positional shift of this core provides an estimate for the magnetic field at one parsec, $B'_{1\text{pc}}$, which we use to derive the poloidal magnetic flux threading parsec-scale jets, Φ_{jet} . This,

by the flux freezing approximation, should be the same as the magnetic flux threading the black hole, Φ_{BH} . We compare Φ_{jet} to the predicted amount of magnetic flux corresponding to a magnetically arrested disk, $50 \left(\dot{M} r_g^2 c \right)^{1/2} \propto L_{\text{acc}}^{1/2} M$, where L_{acc} is the accretion disk luminosity. Γ is the jet bulk Lorentz factor and characterizes the jet velocity. This figure makes use of data from the MOJAVE database (<http://www.physics.purdue.edu/astro/mojave/>).

¹Max-Planck-Institut für Radioastronomie, Auf dem Hügel 69, 53121 Bonn, Germany. ²Lawrence Berkeley National Laboratory, 1 Cyclotron Road, Berkeley, California 94720, USA. ³Department of Astronomy and Theoretical Astrophysics Center, University of California, Berkeley, California 94720-3411, USA.

scales as $50 \left(\dot{M} r_g^2 c \right)^{1/2} \propto L_{\text{acc}}^{1/2} M$, where L_{acc} is the accretion disk luminosity. The disk luminosity enters this relation via the radiative efficiency η , where $L_{\text{acc}} = \eta \dot{M} c^2$; in this work we use $\eta = 0.4$ (see Methods for details).

We test the magnetically arrested disk model by plotting the values of Φ_{jet} versus $L_{\text{acc}}^{1/2} M$ for a sample of radio-loud AGN with measured core-shifts and accretion disk luminosities. If all sources contain magnetically arrested disks, then the data in this plot will display two qualities: (1) there will be a positive correlation between Φ_{jet} and $L_{\text{acc}}^{1/2} M$, and (2) the data points will be scattered around the theoretical curve defined by the relation $\Phi_{\text{jet}} \approx 50 \left(\dot{M} r_g^2 c \right)^{1/2}$.

We use measured core-shifts from a sample of 191 radio-loud AGN¹³ and from individual nearby sources^{12,14–18} (see Extended Data Tables 1 and 2). We have also searched the literature for available estimates of black hole mass for the above-mentioned radio sources and found reliable estimates for 76 of them (see Methods). The masses are estimated assuming that the dynamics of the broad line region around the central black hole are governed by the black hole's gravity. Well-established empirical correlations are then used to relate the observed luminosity of the optical lines to the size of the broad line region, while line widths are used to estimate the gas velocity in this region. From the size and velocity estimates the virial mass for the central body can be calculated^{19–21}. We have also used reported^{19–22} broad line luminosities as a proxy for the accretion disk luminosities, L_{acc} .

We calculate Φ_{jet} and $L_{\text{acc}}^{1/2} M$ for each source in our sample, assuming $a_* = 1.0$, and plot our results in Fig. 2. A partial Kendall correlation test between Φ_{jet} and $L_{\text{acc}}^{1/2} M$, considering the common dependence of these two quantities on redshift and mass, confirms a positive correlation (over 3σ significance), which is not an artefact caused by either distance- or mass-driven selection biases (see Methods and Extended Data Tables 3 and 4 for more details). The scatter in this correlation may be caused by deviations from our assumptions that $a_* = 1$ and $\eta = 0.4$, as well as by observational errors. For example, most black hole spins are predicted²³ to fall in the range $0.3 \lesssim a_* \leq 1$, and η may be different for each source, especially for low-luminosity AGN in our sample which are expected²⁴ to have $\eta \ll 0.4$. Given that our sample is made up of diverse sources with different accretion histories, this correlation might seem surprising. However, magnetically arrested disk theory nicely explains this because it predicts a saturation value of magnetic flux that is mostly independent of initial conditions¹⁰.

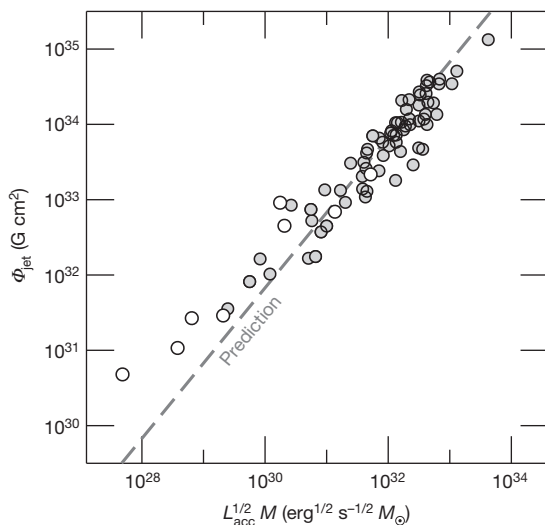


Figure 2 | Measured magnetic flux of the jet, Φ_{jet} , versus $L_{\text{acc}}^{1/2} M$. Here we assume that $\Gamma\theta_j = 1$; we also assume an accretion radiative efficiency of $\eta = 0.4$ for our sample of 76 sources. The dashed line shows the theoretical prediction based on the magnetically arrested disk model. Filled and open circles represent blazars and radio galaxies, respectively (see Methods for details).

We fit the equation $\Phi_{\text{jet}} = \phi_{\text{BH}} \left(\dot{M} r_g^2 c \right)^{1/2}$ to the data by varying the dimensionless free parameter ϕ_{BH} , which can be interpreted as a dimensionless magnetic flux and is predicted to be $\phi_{\text{BH}} \approx 50$ for magnetically arrested disks. We find a best fit, $\phi_{\text{BH}} = (52 \pm 5) \Gamma\theta_j$, where the error is the 1σ confidence interval. The best fit value for ϕ_{BH} is expressed in terms of $\Gamma\theta_j$ because this value is not well known. AGN jet launching models²⁵ typically find $\Gamma\theta_j \approx 1$, implying that most of the sources are close to the magnetically arrested disk prediction, $\phi_{\text{BH}} \approx 50$, and their magnetic fields are dynamically important. However, we note that in the less luminous regions of jets that are well downstream of the bright radio core where our magnetic field measurements are taken, the typical value of $\Gamma\theta_j$ is²⁶ 0.1–0.2, which would give $\phi_{\text{BH}} \approx 10$ for most sources. Even if this low value of $\Gamma\theta_j$ holds in the radio cores, it would still imply that a fraction of the sources, including the M87 galaxy, have dynamically important magnetic fields near their central black holes. Because our magnetic field measurements use emission located closer to the jet launching regions, we assume $\Gamma\theta_j \approx 1$ as predicted by jet launching models, and therefore $\phi_{\text{BH}} \approx 50$ in agreement with magnetically arrested disk predictions. Thus, our data confirm the magnetically arrested disk model because it displays, as discussed above, a positive correlation between Φ_{jet} and $L_{\text{acc}}^{1/2} M$, and the data points are scattered around the theoretical curve defined by $\Phi_{\text{jet}} \approx 50 \left(\dot{M} r_g^2 c \right)^{1/2}$.

Our data provide direct observational evidence that the inner accretion disks of radio-loud AGN contain strong, dynamically important magnetic fields regulated by the mass accretion rate. As most models of black hole accretion disks rely on the assumption that the magnetic pressure in the disk body is much less than the plasma pressure, our findings imply that these models may require significant changes. In particular, attempts to model the silhouette of the central black hole in the M87 galaxy and the spectral energy distributions of X-ray binaries hosting strong radio jets may be in need of significant revision. Models of the Galactic Centre accretion disk may also need to be revised, as a dynamically important magnetic field has been reported⁵ within a distance of $\sim 3 \times 10^7 r_g$ from the central black hole.

The quantitative agreement between Φ_{jet} and $50 \left(\dot{M} r_g^2 c \right)^{1/2}$ demonstrates that our current theoretical models of magnetically arrested disks capture the most important processes in the accretion flow responsible for jet formation. This also implies that most, if not all, radio-loud objects contain dynamically important magnetic flux near their central black holes and that it is the magnetic fields twisted by the rotation of these black holes that power their jets (that is, the Blandford–Znajek mechanism²). These twisted large-scale magnetic fields transfer energy (in the form of Poynting flux) from the rotating black holes out to parsec-scale distances, where their strength can be estimated by the core-shift effect. Our results are consistent with the proposal that radio-loud AGN consist of those black hole systems whose environment/accretion history is conducive to the formation of magnetically arrested disks, whereas radio-quiet AGN (that is, AGN without powerful jets) have failed to form magnetically arrested disks²⁷. The idea that radio-quiet AGN are failed magnetically arrested disks is bolstered by the few studies of black hole spin made for radio-quiet AGN²⁸, which find close to maximally spinning black holes, implying that the Blandford–Znajek power (which presumably controls radio-loudness) must be low due to low magnetic flux threading their black holes. The importance of black hole feedback in part depends on jet power, which is typically assumed^{29,30} to be $\sim 0.1 \dot{M} c^2$. However, our findings imply that much higher jet powers of $\sim \dot{M} c^2$ are common³, hence suggesting that jets play a more important role in the process of AGN feedback than typically assumed.

METHODS SUMMARY

Our sample consists of two types of source: (1) blazars (68 sources), which are AGN with jets directed almost at Earth such that their emission is significantly boosted by relativistic effects, and (2) nearby radio galaxies (8 sources), which are AGN with jets that are typically more closely aligned with the plane of the sky.

To obtain Φ_{jet} for each source, we use published measurements of the core-shift, which is the angular distance that the radio core of each source shifts on the sky when observed at different frequencies using very long baseline interferometry (VLBI). We calculate the jet co-moving frame magnetic field strength one parsec downstream of the black hole, B'_{pc} , by using standard theoretical assumptions about the radio core's emission and absorption mechanism (the synchrotron process), the ratio of magnetic energy to particle energy, and the flux freezing approximation¹². The results of analytical and numerical models of jets^{2,3} are then used to calculate Φ_{jet} from B'_{pc} .

For each source, we calculate \dot{M} from the L_{acc} value derived from that source's line luminosities (H β or Mg II or O III), assuming that all the sources in our sample have the same radiative efficiency of $\eta = 0.4$. Although there are theoretical arguments that magnetically arrested disks could have slightly higher or lower η , our results are not particularly sensitive to the assumed value of η because the value of ϕ_{BH} , which we set out to measure, is proportional to $\eta^{1/2}$.

The correlation we find between Φ_{jet} and $L_{\text{acc}}^{1/2} \dot{M}$ (in excess of 3σ) accounts for all of our data including a number of upper limits. We quantify the scatter in our correlation by finding the two theoretical curves defined by ϕ_{BH} that encompass the middle 68% of our data, which gives $\phi_{\text{BH}} = 24$ and $\phi_{\text{BH}} = 93$.

Online Content Any additional Methods, Extended Data display items and Source Data are available in the online version of the paper; references unique to these sections appear only in the online paper

Received 13 January; accepted 14 April 2014.

- Meier, D. L. *Black Hole Astrophysics: The Engine Paradigm* (Springer, 2012).
- Blandford, R. D. & Znajek, R. L. Electromagnetic extraction of energy from Kerr black holes. *Mon. Not. R. Astron. Soc.* **179**, 433–456 (1977).
- Tchekhovskoy, A., Narayan, R. & McKinney, J. C. Efficient generation of jets from magnetically arrested accretion on a rapidly spinning black hole. *Mon. Not. R. Astron. Soc.* **418**, L79–L83 (2011).
- Balbus, S. A. & Hawley, J. F. A powerful local shear instability in weakly magnetized disks. I. Linear analysis. *Astrophys. J.* **376**, 214–222 (1991); A powerful local shear instability in weakly magnetized disks. II. Nonlinear evolution. *Astrophys. J.* **376**, 223–233 (1991).
- Eatough, R. P. *et al.* A strong magnetic field around the supermassive black hole at the centre of the Galaxy. *Nature* **501**, 391–394 (2013).
- Narayan, R., Igumenshchev, I. V. & Abramowicz, M. A. Magnetically arrested disk: an energetically efficient accretion flow. *Publ. Astron. Soc. Jpn* **55**, L69–L72 (2003).
- McKinney, J. C., Tchekhovskoy, A. & Blandford, R. D. General relativistic magnetohydrodynamic simulations of magnetically choked accretion flows around black holes. *Mon. Not. R. Astron. Soc.* **423**, 3083–3117 (2012).
- McKinney, J. C., Tchekhovskoy, A. & Blandford, R. D. Alignment of magnetized accretion disks and relativistic jets with spinning black holes. *Science* **339**, 49–52 (2013).
- Tchekhovskoy, A., McKinney, J. C. & Narayan, R. General relativistic modeling of magnetized jets from accreting black holes. *J. Phys. Conf. Ser.* **372**, 012040 (2012).
- Tchekhovskoy, A. & McKinney, J. C. Prograde and retrograde black holes: whose jet is more powerful? *Mon. Not. R. Astron. Soc.* **423**, L55–L59 (2012).
- Sikora, M., Stawarz, L. & Lasota, J.-P. Radio loudness of active galactic nuclei: observational facts and theoretical implications. *Astrophys. J.* **658**, 815–828 (2007).
- Lobanov, A. P. Ultracompact jets in active galactic nuclei. *Astron. Astrophys.* **330**, 79–89 (1998).
- Pushkarev, A. B. *et al.* MOJAVE: Monitoring of jets in active galactic nuclei with VLBA experiments. IX. Nuclear opacity. *Astron. Astrophys.* **545**, A113 (2012).
- Kovalev, Y. Y., Lobanov, A. P., Pushkarev, A. B. & Zensus, J. A. Opacity in compact extragalactic radio sources and its effect on astrophysical and astrometric studies. *Astron. Astrophys.* **483**, 759–768 (2008).
- Müller, C. *et al.* Dual-frequency VLBI study of Centaurus A on sub-parsec scales. The highest-resolution view of an extragalactic jet. *Astron. Astrophys.* **530**, L11 (2011).
- Kadler, M., Ros, E., Lobanov, A. P., Falcke, H. & Zensus, J. A. The twin-jet system in NGC 1052: VLBI-scrutiny of the obscuring torus. *Astron. Astrophys.* **426**, 481–493 (2004).
- Hada, K. *et al.* An origin of the radio jet in M87 at the location of the central black hole. *Nature* **477**, 185–187 (2011).
- Marti-Vidal, I. *et al.* Detection of jet precession in the active nucleus of M81. *Astron. Astrophys.* **533**, A111 (2011).
- Kaspi, S. *et al.* Reverberation measurements for 17 quasars and the size-mass-luminosity relations in active galactic nuclei. *Astrophys. J.* **533**, 631–649 (2000).
- Woo, J.-H. & Urry, C. M. Active galactic nucleus black hole masses and bolometric luminosities. *Astrophys. J.* **579**, 530–544 (2002).
- Liu, Y., Jiang, D. R. & Gu, M. F. The jet power, radio loudness, and black hole mass in radio-loud active galactic nuclei. *Astrophys. J.* **637**, 669–681 (2006).
- Punsly, B. & Zhang, S. Calibrating emission lines as quasar bolometers. *Mon. Not. R. Astron. Soc.* **412**, L123–L127 (2011).
- Volonteri, M., Sikora, M., Lasota, J.-P. & Merloni, A. The evolution of active galactic nuclei and their spins. *Astrophys. J.* **775**, 94 (2013).
- Ho, L. C. Nuclear activity in nearby galaxies. *Annu. Rev. Astron. Astrophys.* **46**, 475–539 (2008).
- Komisarov, S. S., Vlahakis, N., Königl, A. & Barkov, M. V. Magnetic acceleration of ultrarelativistic jets in gamma-ray burst sources. *Mon. Not. R. Astron. Soc.* **394**, 1182–1212 (2009).
- Clausen-Brown, E., Savolainen, T., Pushkarev, A. B., Kovalev, Y. Y. & Zensus, J. A. Causal connection in parsec-scale relativistic jets: results from the MOJAVE VLBI survey. *Astron. Astrophys.* **558**, A144 (2013).
- Sikora, M. & Begelman, M. C. Magnetic flux paradigm for radio loudness of active galactic nuclei. *Astrophys. J.* **764**, L24–L28 (2013).
- Fabian, A. C. *et al.* Broad line emission from iron K- and L-shell transitions in the active galaxy 1H0707–495. *Nature* **459**, 540–542 (2009).
- McKinney, J. C. Total and jet Blandford-Znajek power in the presence of an accretion disk. *Astrophys. J.* **630**, L5–L8 (2005).
- Hawley, J. F. & Krolik, J. H. Magnetically driven jets in the Kerr metric. *Astrophys. J.* **641**, 103–116 (2006).

Acknowledgements We thank A. Lobanov, M. Sikora and J. McKinney for discussions and N. Sabha for comments on the manuscript. M.Z. was supported by the German Deutsche Forschungsgemeinschaft, DFG, via grant SFB 956 project A2. A.T. was supported by a Princeton Center for Theoretical Science fellowship and by NASA through the Einstein fellowship program, grant PF3-140115.

Author Contributions M.Z. proposed the experiment, compiled the data and performed most of the analysis. E.C.-B. wrote most of the main text and contributed to the theoretical analysis and implications of the work. T.S. contributed to the analysis and discussion of the data, and A.T. contributed to the theoretical analysis and implications of the work. All authors contributed ideas, discussed the results and wrote the manuscript.

Author Information Reprints and permissions information is available at www.nature.com/reprints. The authors declare no competing financial interests. Readers are welcome to comment on the online version of the paper. Correspondence and requests for materials should be addressed to M.Z. (m.zamaninasab@gmail.com).

METHODS

Data. Our sample of radio-loud AGN can be subdivided into two classes of objects: blazars and nearby radio galaxies. Extended Data Table 1 lists the properties of 68 blazars in our sample, including several well studied ones (3C 454.3, 3C 279 and BL Lac)¹⁵. We searched the literature and found optical line observations that we used to calculate the mass of the corresponding black holes and the bolometric luminosities of their accretion disks.

Extended Data Table 2 lists the same properties as Extended Data Table 1, but for nearby radio galaxies that have core-shifts and accretion disk luminosities reported in the literature (we found only eight such cases). Core-shift measures are taken from different individual experiments: NGC 1052¹⁶, 3C 120¹⁴, M 81¹⁸, W Comae¹⁴, M 87¹⁷, Cen A¹⁵, 3C 390.3¹⁴ and Cyg A¹². Owing to their proximity, six of these objects have black hole masses measured either via stellar velocity dispersion/nuclear gas dynamics modelling (NGC 1052, M 81, M 87, Cen A, Cyg A) or reverberation mapping (3C 120).

Calculating the jet poloidal magnetic flux from the core-shift measure. According to the standard model of relativistic jets³¹, the observed position of the radio core (a bright, synchrotron self-absorbed emission feature at the upstream end of the jet) is a function of the observing frequency. This frequency-dependent shift in the location of the core can be used to estimate the magnetic field strength and electron number density^{12,32}. The method is based on several simple and reasonable assumptions: the flow has a conical shape with a small half-opening angle, θ_j , and constant Γ (no significant acceleration or deceleration). Furthermore, the magnetic field strength and electron number density are assumed to decrease with increasing distance from the central engine following power-law dependencies: $B'(z) = B'_{1\text{pc}}(z/1\text{pc})^{-z_b}$, $n'_e(z) = n'_{e,1\text{pc}}(z/1\text{pc})^{-z_n}$ where z is the distance from the black hole (see Fig. 1). Here $B'_{1\text{pc}}$ and $n'_{e,1\text{pc}}$ represent the jet frame magnetic field strength and electron number density at distance of one parsec away from the apex of the jet. These assumptions lead to a power-law behaviour¹² for the amount of core-shift as a function of the observing frequency, $\propto \nu^{-1/k_r}$, where k_r is the core-shift index. We calculate the core-shift using¹²:

$$\Omega_{rv} = 4.85 \times 10^{-9} \left[\frac{\Delta r_{\text{core}, \nu_1 \nu_2} D_L}{(1+z_*)^2} \right] \left[\frac{v_1^{1/k_r} v_2^{1/k_r}}{v_2^{1/k_r} - v_1^{1/k_r}} \right] \text{pc GHz} \quad (2)$$

where $\Delta r_{\text{core}, \nu_1 \nu_2}$, D_L and z_* are the observed shift (in milliarcsec) of the core position between frequencies ν_1 and ν_2 (in GHz), the luminosity distance, and redshift of the source respectively (note we use z_* for redshift to distinguish it from the cylindrical coordinate z).

If the magnetic field decays with distance as z^{-1} as expected for an azimuthally dominated magnetic field, and the magnetic to non-thermal particle energy ratio remains constant, then it is expected that $k_r = 1$. Numerous observations have indeed revealed a $k_r = 1$ behaviour of the core-shift, thus supporting our assumption of a azimuthally dominated magnetic field in the radio core region^{14,33,34}. Assuming equipartition between magnetic and particle energy at the position of the radio core, then with the above assumptions for the scaling of the magnetic field and relativistic electron density with distance, one can estimate the jet frame magnetic field strength at 1 pc from the black hole:

$$B'_{1\text{pc}} \approx 0.025 \left[\frac{\sigma_{\text{rel}} \Omega_{rv}^3 (1+z_*)^2}{\theta_j \delta^2 \sin^2 \theta} \right]^{0.25} \quad (3)$$

where δ and θ are the Doppler factor and the viewing angle of the jet, respectively. It is assumed that the source has a spectral index of $\alpha = -0.5$. Here σ_{rel} is the ratio of the energy density in the magnetic field to the energy density in the non-thermal relativistic particles responsible for jet emission. We assume equipartition such that $\sigma_{\text{rel}} = 1$, though if this assumption is incorrect it would not strongly affect our results because the jet magnetic flux goes as $\Phi_{\text{jet}} \propto \sigma_{\text{rel}}^{1/4}$.

For the estimate of the magnetic field we assume that (when a good estimate of the viewing angle is not available) jets of this sample of blazars are viewed close to their critical angle¹³, $\theta \approx \Gamma^{-1}$. We compared a sub-sample of 32 sources with known Doppler factors³⁵ and viewing and intrinsic opening angles^{26,36,37} and found this is in fact a reasonable assumption for this sample. This yields¹³:

$$B'_{1\text{pc}} \approx 0.042 \Omega_{rv}^{3/4} (1+z_*)^{1/2} \left(1 + \beta_{\text{app}}^2 \right)^{1/8} \quad (4)$$

where β_{app} is the characteristic apparent speed of a jet's components.

We assume the mean jet frame magnetic field measured in the radio core is predominantly azimuthal, as expected in magnetically powered relativistic jets³⁸⁻⁴⁰. As discussed above, this assumption is supported by the findings from core-shift studies that $k_r = 1$, as well as other VLBI studies³³ of jets that are consistent with a $B \propto z^{-1}$ scaling, which is the expected scaling for a azimuthally dominated magnetic field in a conical jet. Theoretically, in Blandford-Znajek jets the azimuthal to poloidal field

ratio is $B_\phi/B_p \approx R_j/R_{\text{LC}} \approx a_* R_j / [(4-8)r_g]$, which clearly is much greater than unity on VLBI scales². This ratio was calculated for a rapidly spinning black hole ($a_* \approx 1$), and $R_{\text{LC}} = c/\Omega_F$ is the radius of the light cylinder, where Ω_F is the angular frequency of magnetic field lines that remains constant along the jet (it is probably^{3,41,42} between 1/4 and 1/2 of the black hole angular frequency $\Omega_H = ca_*/(2r_H)$).

Let us consider a representative field line in the bulk of the jet, where most of the energy flows out and the observer frame magnetic field is strongest. In an idealized case of a highly magnetized jet, the poloidal magnetic field is approximately uniform over the cross-section of the jet, and we have two familiar relationships: the observer frame azimuthal field scales as $B_\phi \propto R_j^{-1}$, and the poloidal field scales as $B_p \propto R_j^{-2}$, where R_j is the jet cylindrical radius⁴³. Realistic jets are, however, probably not very highly magnetized: the process of jet acceleration requires conversion of Poynting flux to kinetic flux. In this conversion process, B_p becomes non-uniform across the jet^{25,44}. Because of this, B_p decreases faster than R_j^{-2} and B_ϕ decreases faster than R_j^{-1} in the jet acceleration region. The poloidal magnetic field strength B_p along the field line is related⁴⁴ to the total enclosed poloidal magnetic flux in the jet by $\Phi_{\text{jet}} = k\pi R_j^2 B_p$, where $k = (1 - \Gamma/\mu)^{-1} \geq 1$ is the correction factor and Γ is the Lorentz factor of the field line. Here μ is the Lorentz factor that the field line would have if all of the Poynting flux were converted into kinetic energy flux. If we now eliminate B_p in favour of B_ϕ using the relationship in the previous paragraph, we obtain a more general form for equation (1):

$$\Phi_{\text{jet}} = \frac{2\pi(\Gamma\theta_j)r_H z B'_\phi}{\ell a_* (1 - \Gamma/\mu)} \quad (5)$$

where z is the distance down the jet, $B'_\phi = B_\phi/\Gamma$ is the azimuthal magnetic field in the jet frame, and ℓ is defined such that $\Omega_F = \ell\Omega_H$. In order to reproduce equation (1), we assume $z = 1$ pc, $\ell = 1/2$, $\Gamma = \mu/2$, and $B'_\phi \approx B'_{1\text{pc}}$ because the jet co-moving frame magnetic field probed by core-shift measurements on parsec-scales, $B'_{1\text{pc}}$, is likely to be azimuthally dominated. The assumption that $\Gamma = \mu/2$ is justified by different analytical and numerical^{25,44} studies of jet acceleration, which have found that at the end of the acceleration region roughly 50% of a jet's Poynting flux is converted into kinetic energy flux. We convert between jet cylindrical radius R_j and jet downstream distance z by using a conical jet approximation such that $R_j \approx \theta_j z$.

Predicted magnetic flux in a magnetically arrested disk. Under the assumption that the width of the optical broad lines emitted from the clouds surrounding black holes is mainly regulated by the gravitational potential of the black holes (assuming that these ionized clouds follow Keplerian orbits) and using a well-established empirical relation between the size of the broad line region and optical continuum luminosity, one can derive an order of magnitude estimate for black hole masses (for different line diagnostics)^{19,45-50}:

$$M \approx 4.82 \times \left[\frac{\lambda L_{5100\text{\AA}}}{10^{44} \text{ erg s}^{-1}} \right]^{0.69} \left[\frac{\text{FWHM}_{\text{H}\beta}}{\text{km s}^{-1}} \right]^2 M_\odot \quad (6)$$

$$M \approx 3.37 \times \left[\frac{\lambda L_{3000\text{\AA}}}{10^{44} \text{ erg s}^{-1}} \right]^{0.47} \left[\frac{\text{FWHM}_{\text{MgII}}}{\text{km s}^{-1}} \right]^2 M_\odot \quad (7)$$

$$M \approx 33.1 \times \left[\frac{\lambda L_{1350\text{\AA}}}{10^{44} \text{ erg s}^{-1}} \right]^{0.46} \left[\frac{\text{FWHM}_{\text{CIV}}}{\text{km s}^{-1}} \right]^2 M_\odot \quad (8)$$

Here λ is the observed monochromatic continuum luminosity at wavelength λ and $\text{FWHM}_{\text{line}}$ is the observed full-width at half-maximum of the line in question. In radio-loud AGN, the optical emission can be contaminated by the non-thermal synchrotron emission of their jets, so we estimate the optical continuum on the basis of the broad emission line luminosities²¹.

Furthermore, we have used broad (and in two cases narrow) line luminosities as a surrogate for the thermal (non-beamed) emission from the accretion disk. The scaling relations between L_{acc} and the line luminosity, L_{line} , for different lines are^{19,22,51,52}:

$$\log_{10} L_{\text{acc}} = (12.32 \pm 0.32) + (0.78 \pm 0.01) \log_{10} L_{\text{H}\beta} \quad (9)$$

$$\log_{10} L_{\text{acc}} = (16.76 \pm 0.26) + (0.68 \pm 0.01) \log_{10} L_{\text{MgII}} \quad (10)$$

$$\log_{10} L_{\text{acc}} = (26.50 \pm 0.32) + (0.46 \pm 0.01) \log_{10} L_{\text{OIII}} \quad (11)$$

We may now calculate the predicted magnetically arrested disk magnetic flux for a source with known M and L_{acc} :

$$50 \left(\dot{M} r_g^2 c \right)^{1/2} = 2.4 \times 10^{34} \left[\frac{\eta}{0.4} \right]^{-1/2} \left[\frac{M}{10^9 M_\odot} \right] \left[\frac{L_{\text{acc}}}{1.26 \times 10^{47} \text{ erg s}^{-1}} \right]^{1/2} \text{G cm}^2 \quad (12)$$

To calculate \dot{M} from L_{acc} , we assume that all of the sources in our sample have the same radiative efficiency η . If the gravitational binding energy of accreting gas is

radiated away by the time it reaches the black hole's innermost stable orbit, then for a maximally spinning black hole⁵³ $\eta \approx 0.42$. Magnetically arrested disks may behave differently from standard disks, with $\eta \approx 0.5$ for non-rotating black holes and potentially higher η for rotating black holes⁶. The radiative efficiency could be even higher if inverse Compton scattering by the hot, magnetized disk corona reprocesses disk emission. On the other hand, if a fraction of liberated binding energy is carried away mechanically (for example, by magnetized winds) instead of by radiation, the resulting η values could be lower (since the efficiency of magnetized winds in the magnetically arrested disk model is⁹ $\eta \leq 0.2$, we expect this to be at most a modest correction). Note that since the value of ϕ_{BH} , which we set out to measure, is proportional to $\eta^{1/2}$, our results are not particularly sensitive to the assumed value of η . In this work, we adopt a representative value, $\eta = 0.4$.

Linear regression and partial correlation analysis. In order to probe for possible correlations between observed values (for example, accretion luminosity and magnetic field strength), one should take into account their possible common dependencies on other parameters (for example, distance, mass and relativistic boosting). We have done this by using a generalized version of the partial Kendall's τ_K correlation test⁵⁴ that is suitable for our sample (which includes a number of upper limits). We used the publicly available FORTRAN code⁵⁵ which has been widely used for probing correlations in astronomical data sets. Extended Data Table 3 summarizes the results of our partial correlation analysis.

Furthermore, we have double-checked our results with the ppcorr package⁵⁶ which is available as a public library for \mathcal{R}^{57} . The ppcorr package calculates the Kendall τ_K correlation between different observed values while controlling for dependencies on more than one commonly dependent variable. However, ppcorr does not take upper and lower limits (so-called censored data points) into account properly. Extended Data Table 4 summarizes the results of a test using ppcorr for a correlation between Φ_{jet} and $L_{\text{acc}}^{1/2} M$ while simultaneously controlling for common dependencies on mass, redshift and apparent velocity.

The scatter in the observed correlation can be quantified in terms of the free parameter defining the theoretically predicted curves, ϕ_{BH} . If we search for the two theoretical curves that encompass the middle 68% of the data points (that is, 16% of the data lie above the upper line and 16% of the data lie below the lower line), then we find the curves defined by $\phi_{\text{BH}} = 24$ and $\phi_{\text{BH}} = 93$ satisfy this criterion (recall $\phi_{\text{BH}} \approx 50$ is the value predicted by magnetically arrested disk theory). Note that when we state the results of the fit, $\phi_{\text{BH}} = (52 \pm 5)$, the error represents the confidence interval of the best fit value, and does not refer to the scatter discussed above. The best fit value and its confidence interval are obtained using the MPFIT package^{58,59}.

We also performed linear regression between different observed values (for example, Φ_{jet} and $L_{\text{acc}}^{1/2} M$) using a Bayesian method that accurately accounts for the censored data points⁶⁰. For this purpose we have used the LINMIX_ERR routine which is publicly available as a part of the astrolib package⁶¹. We have used the Metropolis-Hastings algorithm available in the code to obtain the posterior distribution. The linear regression results in a best-fit model $\log \Phi_{\text{jet}} = (8.52 \pm 1.06) + (0.79 \pm 0.03) \times \log L_{\text{acc}}^{1/2} M$ (1 σ confidence).

31. Blandford, R. D. & Königl, A. Relativistic jets as compact radio sources. *Astrophys. J.* **232**, 34–48 (1979).
32. Hirovani, K. Kinetic luminosity and composition of active galactic nuclei jets. *Astrophys. J.* **619**, 73–85 (2005).
33. O'Sullivan, S. P. & Gabuzda, D. C. Magnetic field strength and spectral distribution of six parsec-scale active galactic nuclei jets. *Mon. Not. R. Astron. Soc.* **400**, 26–42 (2009).
34. Sokolovsky, K. V., Kovalev, Y. Y., Pushkarev, A. B. & Lobanov, A. P. A VLBA survey of the core shift effect in AGN jets. I. Evidence of dominating synchrotron opacity. *Astron. Astrophys.* **532**, A38 (2011).
35. Hovatta, T., Valtaoja, E., Tornikoski, M. & Lähteenmäki, A. Doppler factors, Lorentz factors and viewing angles for quasars, BL Lacertae objects and radio galaxies. *Astron. Astrophys.* **494**, 527–537 (2009).
36. Pushkarev, A. B., Kovalev, Y. Y., Lister, M. L. & Savolainen, T. Jet opening angles and gamma-ray brightness of AGN. *Astron. Astrophys.* **507**, L33–L36 (2009).
37. Savolainen, T. *et al.* Relativistic beaming and gamma-ray brightness of blazars. *Astron. Astrophys.* **512**, A24 (2010).
38. Gabuzda, D. C., Vitrichchak, V. M., Mahmud, M. & O'Sullivan, S. P. Radio circular polarization produced in helical magnetic fields in eight active galactic nuclei. *Mon. Not. R. Astron. Soc.* **384**, 1003–1014 (2008).

39. Pudritz, R. E., Hardcastle, M. J. & Gabuzda, D. C. Magnetic fields in astrophysical jets: from launch to termination. *Space Sci. Rev.* **169**, 27–72 (2012).
40. Zamaninasab, M. *et al.* Evidence for a large-scale helical magnetic field in the quasar 3C 454.3. *Mon. Not. R. Astron. Soc.* **436**, 3341–3356 (2013).
41. McKinney, J. C. General relativistic magnetohydrodynamic simulations of the jet formation and large-scale propagation from black hole accretion systems. *Mon. Not. R. Astron. Soc.* **368**, 1561–1582 (2006).
42. Tchekhovskoy, A., Narayan, R. & McKinney, J. C. Black hole spin and the radio loud/quiet dichotomy of active galactic nuclei. *Astrophys. J.* **711**, 50–63 (2010).
43. Tchekhovskoy, A., McKinney, J. C. & Narayan, R. Simulations of ultrarelativistic magnetodynamic jets from gamma-ray burst engines. *Mon. Not. R. Astron. Soc.* **388**, 551–572 (2008).
44. Tchekhovskoy, A., McKinney, J. C. & Narayan, R. Efficiency of magnetic to kinetic energy conversion in a monopole magnetosphere. *Astrophys. J.* **699**, 1789–1808 (2009).
45. Wandel, A., Peterson, B. M. & Malkan, M. A. Central masses and broad-line region sizes of active galactic nuclei. I. Comparing the photoionization and reverberation techniques. *Astrophys. J.* **526**, 579–591 (1999).
46. McLure, R. J. & Jarvis, M. J. Measuring the black hole masses of high-redshift quasars. *Mon. Not. R. Astron. Soc.* **337**, 109–116 (2002).
47. Kaspi, S. *et al.* The relationship between luminosity and broad-line region size in active galactic nuclei. *Astrophys. J.* **629**, 61–71 (2005).
48. Greene, J. E. & Ho, L. C. Estimating black hole masses in active galaxies using the H α emission line. *Astrophys. J.* **630**, 122–129 (2005).
49. Shen, Y. *et al.* A catalog of quasar properties from Sloan Digital Sky Survey Data Release 7. *Astrophys. J.* **194**, 45 (2011).
50. Shaw, M. S. *et al.* Spectroscopy of broad-line blazars from 1LAC. *Astrophys. J.* **748**, 49 (2012).
51. Celotti, A., Padovani, P. & Ghisellini, G. Jets and accretion processes in active galactic nuclei: further clues. *Mon. Not. R. Astron. Soc.* **286**, 415–424 (1997).
52. Gu, M., Cao, X. & Jiang, D. R. The bulk kinetic power of radio jets in active galactic nuclei. *Mon. Not. R. Astron. Soc.* **396**, 984–996 (2009).
53. Novikov, I. D. & Thorne, K. S. in *Black Holes* (eds Dewitt, C. & Dewitt, B. S.) 343–450 (Gordon and Breach, Paris, 1973).
54. Akritas, M. G. & Siebert, J. A test for partial correlation with censored astronomical data. *Mon. Not. R. Astron. Soc.* **278**, 919–924 (1996).
55. http://astro.psu.edu/statcodes/cens_tau.f.
56. <http://cran.r-project.org/web/packages/ppcor/index.html>.
57. <http://www.r-project.org>.
58. Markwardt, C. B. in *Astronomical Data Analysis Software and Systems XVIII* (eds Bohlender, D. A., Durand, D. & Dowler, P.) 251–254 (Astron. Soc. Pacif. Conf. Ser. Vol. 411, Astronomical Society of Pacific, 2009).
59. <http://purl.com/net/mpfit>.
60. Kelly, B. C. Some aspects of measurement error in linear regression of astronomical data. *Astrophys. J.* **665**, 1489–1506 (2007).
61. <http://idlastro.gsfc.nasa.gov>.
62. Torrealba, J. *et al.* Optical spectroscopic atlas of the MOJAVE/2cm AGN sample. *Rev. Mex. Astron. Astrofis.* **48**, 9–40 (2012).
63. Palma, N. I. *et al.* Multiwavelength observations of the gamma-ray blazar PKS 0528+134 in quiescence. *Astrophys. J.* **735**, 60 (2011).
64. Di Matteo, T., Allen, S. W., Fabian, A. C., Wilson, A. S. & Young, A. J. Accretion onto the supermassive black hole in M87. *Astrophys. J.* **582**, 133–140 (2003).
65. Evans, D. A. *et al.* Chandra and XMM-Newton observations of the nucleus of Centaurus A. *Astrophys. J.* **612**, 786–796 (2004).
66. Gebhardt, K. *et al.* The black hole mass in M87 from Gemini/NIFS adaptive optics observations. *Astrophys. J.* **729**, 119 (2011).
67. Ghisellini, G. *et al.* General physical properties of bright Fermi blazars. *Mon. Not. R. Astron. Soc.* **402**, 497–518 (2010).
68. González-Martín, O., Masegosa, J., Márquez, I. & Guainazzi, M. Fitting LINER nuclei within the active galactic nucleus family: a matter of obscurity? *Astrophys. J.* **704**, 1570–1585 (2009).
69. King, A. L. *et al.* What is on tap? The role of spin in compact objects and relativistic jets. *Astrophys. J.* **771**, 84 (2013).
70. Markoff, S. *et al.* Results from an extensive simultaneous broadband campaign on the underluminous active nucleus M81*: further evidence for mass-scaling accretion in black holes. *Astrophys. J.* **681**, 905–924 (2008).
71. McNamara, B. R., Rohanizadegan, M. & Nulsen, P. E. J. Are radio active galactic nuclei powered by accretion or black hole spin? *Astrophys. J.* **727**, 39 (2011).
72. Neumayer, N. *et al.* The central parsecs of Centaurus A: high-excitation gas, a molecular disk, and the mass of the black hole. *Astrophys. J.* **671**, 1329–1344 (2007).
73. Kino, M. & Kawakatu, N. Estimate of the total kinetic power and age of an extragalactic jet by its cocoon dynamics: the case of Cygnus A. *Mon. Not. R. Astron. Soc.* **364**, 659–664 (2005).

Extended Data Table 1 | Blazar sample

Object (1)	Type (2)	z_* (3)	β_{app} (c) (4)	$\Omega_{r\nu}$ (pc GHz) (5)	$B'_{1\text{pc}}$ (G) (6)	$\text{Log}_{10} M (M_{\odot})$ (7)	$\text{Log}_{10} L_{\text{acc}}$ (erg s $^{-1}$) (8)	Reference (9)
0133+476	Q	0.86	12.98	13.69	0.77	8.55	46.11	Tor12
0212+735	Q	2.37	7.64	21.24	1.27	9.96	47.33	Tor12
0234+285	Q	1.21	12.26	35.82	1.71	9.22	46.80	Shw12
0333+321	Q	1.26	12.76	41.51	1.95	9.25	47.17	Liu06
0336-019	Q	0.85	22.36	14.41	0.92	8.89	46.33	Liu06
0403-132	Q	0.57	19.69	33.30	1.54	9.08	46.52	Liu06
0420-014	Q	0.91	7.36	35.94	1.41	8.41	46.48	Liu06
0454+844	B	0.11	0.14	10.91	0.27	7.42	44.66	Tor12
0528+134	Q	2.07	19.20	22.71	1.60	9.03	47.23	Pal11
0605-085	Q	0.87	19.79	13.24	0.84	8.87	46.44	Shw12
0607-157	Q	0.32	3.93	21.22	0.68	7.32	45.20	Liu06
0736+017	Q	0.19	14.32	<2.94	<0.20	7.86	45.69	Liu06
0738+313	Q	0.63	10.76	16.85	0.81	9.57	46.93	Liu06
0748+126	Q	0.89	18.37	13.49	0.84	9.06	46.88	Tor12
0804+499	Q	1.44	1.83	11.15	0.48	9.39	46.80	Liu06
0827+243	Q	0.94	22.01	19.64	1.18	8.89	46.46	Tor12
0836+710	Q	2.22	25.38	25.72	1.93	9.36	47.51	Liu06
0859-140	Q	1.34	16.47	30.96	1.70	9.14	46.73	Tor12
0906+015	Q	1.02	20.68	29.45	1.61	8.55	46.61	Liu06
0917+624	Q	1.45	15.57	16.99	1.09	8.93	46.57	Shw12
0923+392	Q	0.69	4.29	<6.64	<0.33	9.09	46.94	Liu06
0945+408	Q	1.25	18.60	17.02	1.10	8.99	46.46	Tor12
0953+254	Q	0.71	11.52	<6.71	<0.42	8.70	46.30	Liu06
1015+359	Q	1.23	12.46	15.55	0.92	8.69	46.65	Tor12
1038+064	Q	1.26	11.87	21.97	1.19	9.12	46.76	Tor12
1127-145	Q	1.18	14.18	13.24	0.84	9.30	46.87	Tor12
1156+295	Q	0.73	24.73	20.11	1.17	8.54	46.25	Liu06
1219+044	Q	0.96	2.35	24.16	0.81	8.89	46.48	Tor12
1222+216	Q	0.43	21.10	17.03	0.90	8.87	46.34	Tor12
1253-055	Q	0.54	20.57	<5.88	<0.42	8.28	46.05	Liu06
1302-102	Q	0.28	5.41	20.34	0.70	8.51	46.26	Liu06
1308+326	Q	1.00	27.17	13.61	0.96	8.72	46.38	Tor12
1334-127	Q	0.54	10.26	31.08	1.23	7.98	45.98	Liu06
1458+718	Q	0.90	7.04	9.46	0.51	9.23	46.80	Liu06
1502+106	Q	1.84	14.77	8.50	0.69	8.74	46.92	Liu06
1508-055	Q	1.19	18.64	26.81	1.52	9.32	46.71	Tor12
1510-089	Q	0.36	20.14	13.50	0.73	8.20	46.05	Liu06
1546+027	Q	0.41	12.08	<5.09	<0.32	8.47	46.32	Liu06
1606+106	Q	1.23	18.91	10.97	0.79	8.97	46.56	Tor12
1611+343	Q	1.40	14.11	9.07	0.66	9.19	46.78	Tor12
1633+382	Q	1.81	29.45	21.21	1.62	9.12	46.80	Tor12
1637+574	Q	0.75	10.61	13.51	0.71	9.22	46.77	Liu06
1641+399	Q	0.59	19.27	23.85	1.20	9.27	46.69	Liu06
1642+690	Q	0.75	16.65	<6.85	<0.48	6.81	45.17	Tor12
1655+077	Q	0.62	14.45	7.45	0.47	7.28	45.60	Liu06
1726+455	Q	0.72	1.82	<6.73	<0.28	9.18	46.63	Tor12
1749+701	B	0.77	6.03	27.03	1.04	8.77	45.96	Tor12
1803+784	B	0.68	8.97	<6.58	<0.39	7.92	45.98	Liu06
1807+698	B	0.05	0.10	3.81	0.12	8.51	44.98	Tor12
1823+568	B	0.66	20.85	11.79	0.74	7.94	45.61	Tor12
1828+487	Q	0.69	13.65	12.24	0.69	8.41	46.34	Tor12
1849+670	Q	0.66	30.63	6.48	0.52	8.81	46.22	Tor12
1901+319	Q	0.63	2.67	29.03	0.87	7.72	46.08	Tor12
1928+738	Q	0.30	8.43	12.31	0.54	8.35	46.47	Liu06
2121+053	Q	1.94	13.29	22.61	1.43	8.78	47.15	Liu06
2128-123	Q	0.50	6.94	26.41	0.98	9.02	46.65	Liu06
2134+004	Q	1.93	5.94	26.23	1.31	9.36	46.93	Tor12
2145+067	Q	0.99	2.52	<7.48	<0.34	8.87	47.07	Liu06
2155-152	Q	0.67	18.11	43.23	1.89	7.59	45.67	Woo02
2200+420	B	0.07	10.57	1.21	0.09	8.23	45.18	Tor12
2201+315	Q	0.29	7.87	27.04	0.95	8.94	46.68	Liu06
2209+236	Q	1.12	3.43	7.69	0.39	8.46	46.39	Shw12
2227-088	Q	1.56	8.14	29.60	1.44	8.98	46.58	Tor12
2230+114	Q	1.04	15.41	46.48	2.12	8.93	46.58	Tor12
2243-123	Q	0.63	5.49	20.10	0.78	8.81	46.64	Tor12
2251+158	Q	0.86	14.19	22.00	0.32	8.69	46.86	Liu06
2345-167	Q	0.58	13.45	18.44	0.90	8.47	45.84	Liu06
2351+456	Q	1.99	18.01	25.97	1.72	9.29	46.68	Tor12

(1), IAU name (B1950); (2), classification of the source (Q, quasar; B, BL Lac object; RG, radio galaxy); (3), redshift; (4), apparent velocity of the jet; (5), core-shift measure; (6), magnetic field strength one parsec away from the jet base; (7), mass of the black hole; (8), accretion disk luminosity; (9), reference for the line used for estimating mass and accretion luminosity. References: Liu06, ref. 21; Tor12, ref. 62; Shw12, ref. 50; Pal11, ref. 63; Woo02, ref. 20.

Extended Data Table 2 | Radio galaxy sample

Object (1)	Type (2)	z_* (3)	β_{app} (c) (4)	$\Omega_{r\nu}$ (pc GHz) (5)	$B'_{1\text{pc}}$ (G) (6)	$\text{Log}_{10} M$ (M_{\odot}) (7)	$\text{Log}_{10} L_{\text{acc}}$ (erg s^{-1}) (8)	Reference (9)
0238–084 (NGC 1052)	RG	0.0050	0.23	0.226	0.015	8.19	41.24	Woo02/Gon09
0430+052 (3C 120)	RG	0.033	4.66	1.85	0.11	7.36	43.92	King13
0951+693 (M 81)	RG	0.0001	1.45	0.031	0.0066	7.80	39.77	Mar08
1219+285 (W Coma)	RG	0.102	4.05	1.39	0.08	8.69	43.25	Ghe10
1228+126 (M 87)	RG	0.004	0.24	0.132	0.012	9.82	40.85	Geb11/DiM03
1322–427 (Cen A)	RG	0.0018	0.50	0.155	0.017	7.74	41.68	Neu09/Eva04
1845+797 (3C 390.3)	RG	0.057	2.29	1.65	0.089	8.83	44.61	Tor12
1957+405 (Cyg A)	RG	0.0562	0.20	2.10	0.07	9.43	44.57	McN11/Kino05

Similar to Extended Data Table 1. References: DiM03, ref. 64; Eva04, ref. 65; Geb11, ref. 66; Ghe10, ref. 67; Gon09, ref. 68; King13, ref. 69; Mar08, ref. 70; McN11, ref. 71; Neu09, ref. 72; Kino05, ref. 73; Tor12, ref. 62; Woo02, ref. 20.

Extended Data Table 3 | Partial correlation analysis results based on cens_tau algorithm

X_1	Variables		X_3	Correlation		Significance of rejecting the null hypothesis
	X_2			τ_K	P_{null}	
All sources:						
$\text{Log } L_{\text{acc}}^{1/2} M$	$\text{Log } \Phi_{\text{jet}}$	z_*	0.62	$< 10^{-13}$	$> 5 \sigma$	
$\text{Log } L_{\text{acc}}^{1/2} M$	$\text{Log } \Phi_{\text{jet}}$	$\text{Log } M$	0.46	1.1×10^{-3}	3.3σ	
$\text{Log } L_{\text{acc}}^{1/2} M$	$\text{Log } \Phi_{\text{jet}}$	β_{app}	0.72	$< 10^{-14}$	$> 5 \sigma$	
Excluding LLAGN:						
$\text{Log } L_{\text{acc}}^{1/2} M$	$\text{Log } \Phi_{\text{jet}}$	z_*	0.61	$< 10^{-13}$	$> 5 \sigma$	
$\text{Log } L_{\text{acc}}^{1/2} M$	$\text{Log } \Phi_{\text{jet}}$	$\text{Log } M$	0.21	1.2×10^{-3}	3.2σ	
$\text{Log } L_{\text{acc}}^{1/2} M$	$\text{Log } \Phi_{\text{jet}}$	β_{app}	0.70	$< 10^{-14}$	$> 5 \sigma$	

X_1 and X_2 are variables that have a possible mutual dependency on variable X_3 . τ_K and P_{null} are the Kendall's partial correlation coefficient and probability for the null hypothesis of no correlation between X_1 and X_2 , respectively. The last column shows the corresponding significance by which the null hypothesis could be rejected.

Extended Data Table 4 | Results of partial correlation analysis based on ppcorr algorithm

	X_1	Variables			X_5	Correlation		Significance of rejecting the null hypothesis
	X_2	X_3	X_4		τ_K	P_{null}		
Excluding upper limits:	$\text{Log } L_{\text{acc}}^{1/2} M$	$\text{Log } \Phi_{\text{jet}}$	z_*	$\text{Log } M$	β_{app}	0.52	1.9×10^{-9}	$> 5 \sigma$
Excluding upper limits and LLGN:	$\text{Log } L_{\text{acc}}^{1/2} M$	$\text{Log } \Phi_{\text{jet}}$	z_*	$\text{Log } M$	β_{app}	0.32	5.2×10^{-3}	3.0σ

X_1 and X_2 are variables that have a possible mutual dependency on variables X_3, X_4 and X_5 . τ_K and P_{null} are the same as in Extended Data Table 3.

Physics and Theory of the Quasi-Coherent Mode**

B. Coppi*

MIT

Presented at the Ignitor Physics Meeting, Rome, April 3, 2014 and at the Sherwood Theory Meeting, San Diego, CA, March 24, 2014. *With a contribution by T. Zhou. **Sponsored in part by the U.S. Department of Energy.

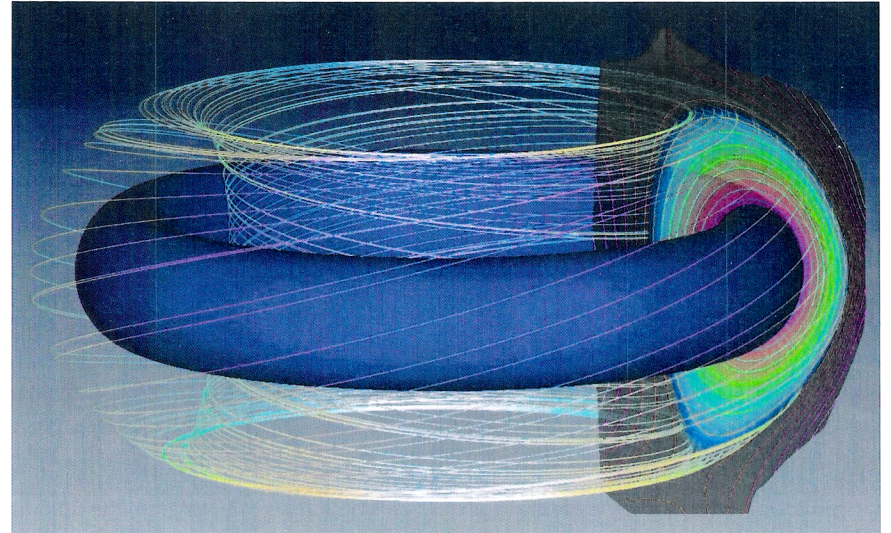
Toroidal magnetic field lines

Axisymmetric D-shaped tokamak with magnetic X-point(s) on separatrix.

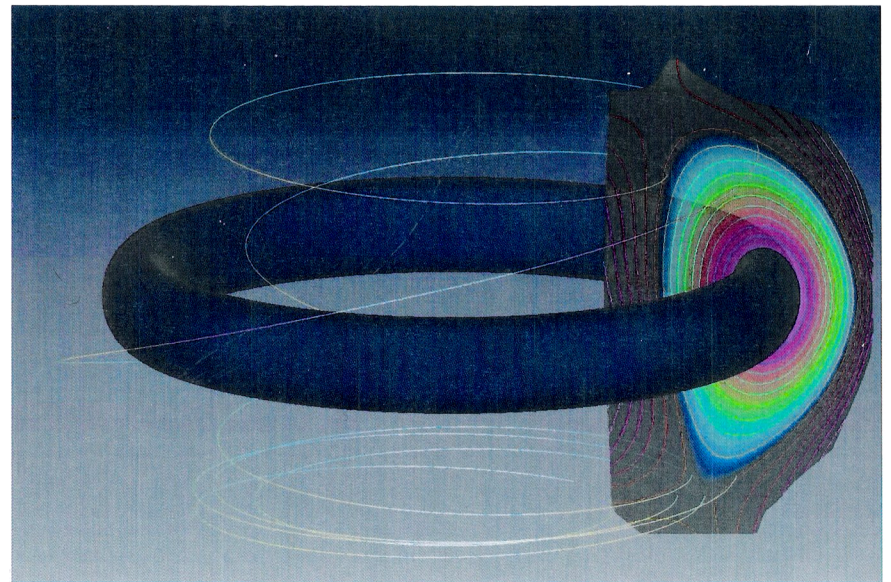
Field line winding number $\bar{l}(\psi)$ varies continuously from $q \approx 1$ ($\bar{l} = 1/q$) to plasma edge (0 on X-point separatrix).

Locally, field lines do most toroidal winding on top/bottom and inboard side of flux surface

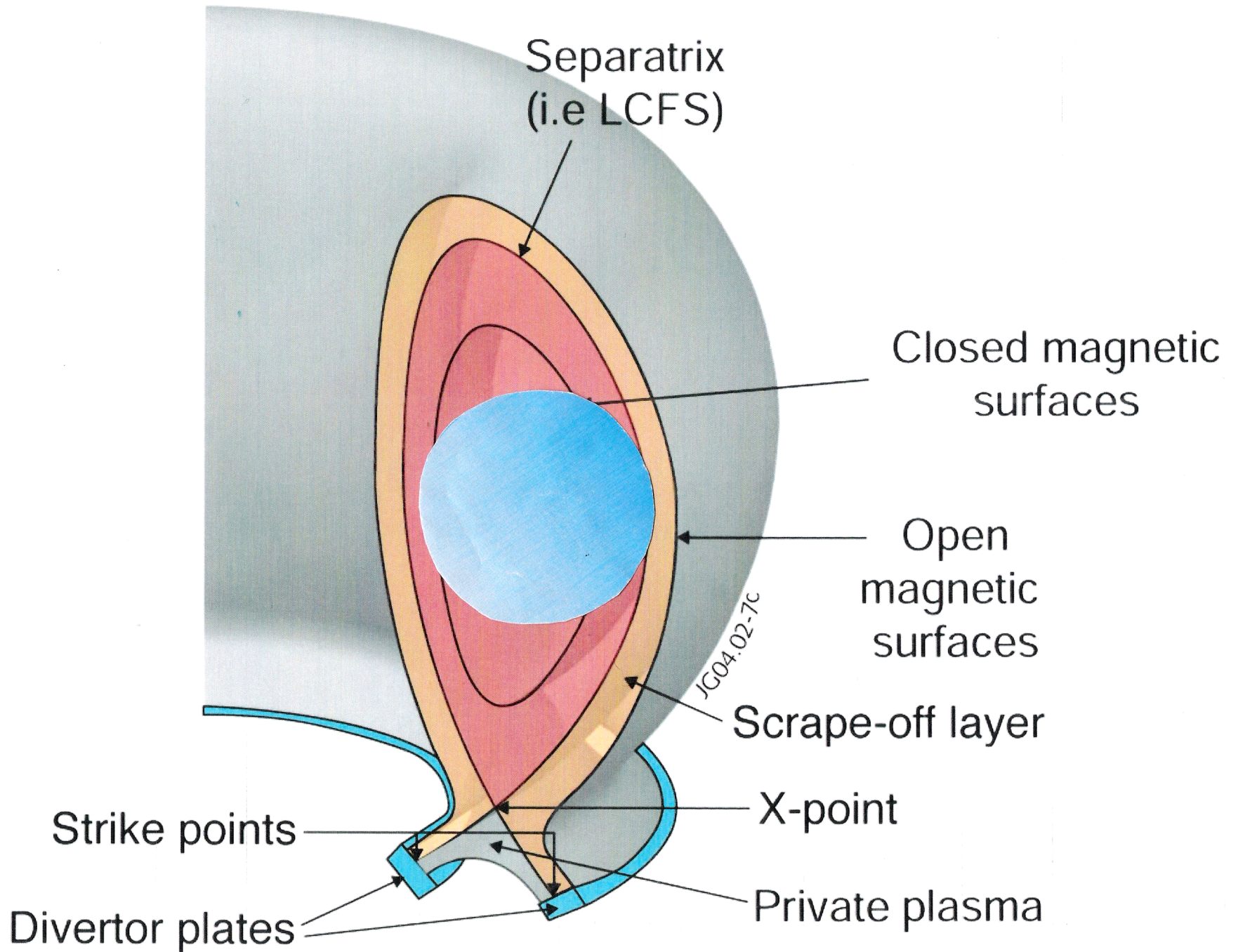
Outboard side: from $q \approx 1$ to beyond separatrix, there is a vertical range centered on the midplane where the field lines have a fairly similar, finite pitch – $B_\theta/B_\phi \approx \text{constant}$ for C-Mod, DIII-D where $a/R \approx 1/3$.



Just inside separatrix (DIII-D, lower X-pt)



Just outside separatrix



Model Field Configuration

$$\mathbf{B} \simeq \frac{B_0 \mathbf{e}_\varphi + B_p(r_s) \mathbf{e}_\theta}{1 + (r/R_0) \cos \theta}$$

$$\frac{B_p(r_s)}{B_0} \simeq \text{const. for } -\theta_0 \leq \theta \leq \theta_0$$

$$\hat{n} \simeq \tilde{n}(r - r_s, \theta) \exp \left\{ -i\omega t + in^0 [\varphi - q(r)\theta] + in^0 [q(r) - q(r_s)] F_c(\theta - \theta_0) \right\}$$

$F_c(\theta)$ = correcting function acting at $\theta \simeq \pm\theta_0$

so that

$$\tilde{n}(r - r_s, \theta \geq \theta_0, \theta \leq -\theta_0) = 0$$

“2-D Ballooning” Modes

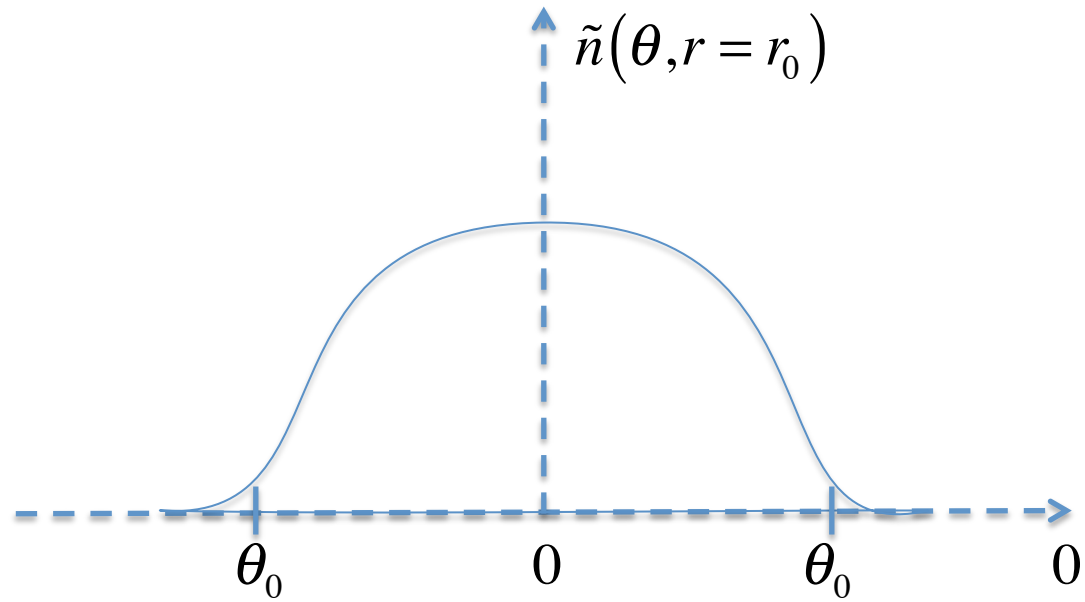
$$\tilde{n} \simeq \tilde{n} \left(\frac{r - r_s}{\delta_r} \right) \cos \left(\frac{\theta - \theta_0}{2} \right) F_c(r - r_s, \theta - \theta_0)$$

for

$$-\theta_0 < \theta < \theta_0$$

$$\frac{\partial^2}{\partial \ell^2} \simeq \left(\frac{B_\theta}{B r_s} \right)^2 \frac{\partial^2}{\partial \theta^2} \simeq -k_\parallel^2$$

$$k_\parallel^2 = \frac{B_\theta^2}{r_s^2 B^2} \left(\frac{1}{\theta_0} \frac{\pi}{2} \right)^2$$



For

$$-\theta_0 + \Delta\theta_0 < \theta \leq \theta_0 - \Delta\theta_0$$

$$\tilde{n} \propto \cos\left(\frac{\pi \theta}{2 \theta_0}\right)$$

“2-D Ballooning” Mode

- Simplified model
- Electrostatic Approximation
- Guiding Center Point of View

$$\hat{\Phi} \simeq \tilde{\phi}(x, \ell) \exp(-i\omega t +iky)$$

$$x = r - r_s$$

$$0 \simeq -\frac{\partial}{\partial \ell} \left(\hat{n}_e T_e + n_e \hat{T}_e - en \hat{\Phi} \right) - v_{ei}^{\parallel} m_e n \hat{u}_{e\parallel}$$

$$-i\omega\hat{n}_e + \hat{V}_{Ex} \frac{\partial n}{\partial r} + n \frac{\partial}{\partial \ell} \hat{u}_{e\parallel} \simeq 0$$

$$\frac{3}{2} \left(-i\omega\hat{T}_e + \hat{V}_{Ex} \frac{dT_e}{dr} \right) + T_e \frac{\partial}{\partial \ell} \hat{u}_{e\parallel} \simeq 0$$

$$-i \left(\omega - k \frac{g_i}{\Omega_{ci}} \right) \hat{n}_i + \hat{V}_{Ex} \frac{dn}{dr} + n \nabla \cdot \left(\hat{\mathbf{V}}_{Pi} + \hat{\mathbf{V}}_{FLR} \right) \simeq 0$$

where

$$g_i \simeq \frac{V_{thi}^2}{R_c}$$

$$x \equiv r - r_s$$

$$\hat{V}_{Ex} = -\frac{1}{r_s} \frac{\partial}{\partial \theta} \hat{\Phi} \frac{c}{B}$$

$$\Omega_{ci} = \frac{eB}{m_i c}$$

$$\frac{\partial}{\partial \ell} = \frac{\mathbf{B}}{B} \cdot \nabla$$

$$\hat{V}_{Pi} = \text{polarization drift} \quad \frac{c}{\Omega_{ci} B} \frac{d\hat{\mathbf{E}}_{\perp}}{dt}$$

$$\hat{\mathbf{V}}_{FLR} \simeq \frac{\omega_{di}}{\omega} \hat{\mathbf{V}}_{Pi} \quad \text{Finite Larmor Radius Drift}$$

Other Definitions

$$\eta_e \equiv \frac{d \ln T_e}{dx} \bigg/ \frac{d \ln n}{dx}$$

$$\omega_{*e} \equiv -k_y \frac{c T_e}{e B n} \frac{dn}{dx}$$

$$\omega_{di} \equiv k_y \frac{c}{e B n} \frac{dp_i}{dx}$$

Then

$$\hat{n}_i \simeq -k \frac{c}{B} \hat{\Phi} \frac{\partial n}{\partial x} \bigg|_0 \frac{1}{\omega} \left(1 + k \frac{g_i}{\omega \Omega_{ci}} \right) + \frac{n}{i\omega} \nabla \cdot \left(\hat{\mathbf{V}}_{Pi} + \hat{\mathbf{V}}_{FLR} \right)$$

$$\hat{n}_e \simeq -\frac{k c}{\omega B} \hat{\Phi} \frac{\partial n}{\partial x} + \frac{n}{i\omega} \frac{\partial}{\partial \ell} \hat{u}_{e\parallel} = \frac{\omega_{*e}}{\omega} \frac{e \hat{\Phi}}{T_e} n + \frac{n}{i\omega} \frac{\partial}{\partial \ell} \hat{u}_{e\parallel}$$

$$\frac{\partial}{\partial \ell} \hat{u}_{e\parallel} \simeq \nabla \cdot \left(\hat{\mathbf{V}}_{Pi} + \hat{\mathbf{V}}_{FLR} \right) - i \frac{k^2 c}{\omega B} \hat{\Phi} \frac{g_i}{\Omega_{ci}^n} \frac{\partial n}{\partial x} \bigg|_0$$

$$v_{ei}^{\parallel} n m_e \frac{\partial}{\partial \ell} \hat{u}_{e\parallel} \simeq -\frac{\partial^2}{\partial \ell^2} \left(\hat{n}_e T_e + n \hat{T}_e - e \hat{\Phi} n \right)$$

Relevant Asymptotic Limits

$$\left| \frac{\partial^2}{\partial r^2} \right| \gg \frac{m^0{}^2}{r_s^2}$$

$$\gamma_G^2 \simeq \frac{V_{thi}^2 (1 + T_i/T_e)}{R_c} \left| \frac{1}{p} \frac{dp}{dr} \right|$$

$$-\frac{1}{r_p} \equiv \frac{1}{p} \frac{dp}{dr}$$

$$\left| \omega_{*e}^p \omega_{di} \right| \ll \gamma_G^2$$

$$\left(\frac{m^0}{r_s}\right) \rho_s \frac{V_s}{r_{pe}} \frac{\rho_i}{2} \frac{V_{thi}}{r_{pi}} \ll \gamma_G^2$$

Roughly

$$\left(\frac{m^0}{r_s}\right)^2 \rho_i^2 \ll \frac{r_p}{R_c}$$

Assume

$$\omega(\omega - \omega_{di}) \frac{\partial^2}{\partial r^2} \sim \frac{m^{0,2}}{r_s^2} \gamma_G^2$$

$$\delta_G^2 \sim \rho_i^2 \frac{R_c}{r_p}$$

Plane Model

$$\mathbf{B} \simeq B_0 \mathbf{e}_z$$

$$\mathbf{g} = g \mathbf{e}_x$$

$$dp/dx \simeq -p(x=0)/r_p$$

$$\hat{\Phi} \simeq \tilde{\phi}(x) \exp(-i\omega t + ik_y y + ik_{\parallel} z)$$

Then

$$\omega \simeq \omega_{TT} \equiv \omega_{*e} \left[1 + (1 + \alpha_T) \eta_T \right]$$

$$\omega \simeq \omega_{TT}^0 + \delta\omega$$

$$\delta\omega = i\gamma + \delta\omega_R$$

$$x = r - r_s, \quad \eta_T = \frac{d \ln T_e}{dr} / \frac{d \ln}{dr}, \quad \omega_{TT} \simeq \omega_{TT}^0 \left(1 - \frac{x^2}{\Delta_x^2} \right)$$

$$\left(\frac{\delta \omega}{\omega_{TT}^0 \epsilon_v} + \frac{x^2}{\Delta_x^2 \epsilon_v} \right) \tilde{\phi}(x) \simeq i \left[1 - \delta_G^2 \frac{d^2}{dx^2} \right] \tilde{\phi}(x)$$

$$\tilde{\phi}(x) \propto \exp\left(-\sigma \frac{x^2}{2}\right)$$

where $\sigma = \sigma_R + i\sigma_I$ and $\sigma_R > 0$. Then

$$\gamma \simeq \epsilon_v \omega_{TT}^0 \left[1 + \frac{\delta_G}{|2\epsilon_v|^{1/2} \Delta_x} \right]$$

where

$$\epsilon_v \omega_{TT}^0 \equiv k_y^2 \rho_s^2 \frac{v_{ei}^{\parallel} m_e}{k_{\parallel}^2 T_e} \gamma_G^2$$

and

$$\gamma_G^2 \equiv \frac{g}{r_p}$$

Moreover

$$\delta_G^2 \equiv \frac{\omega_{TT}^0 (\omega_{TT}^0 - \omega_{di})}{k_y^2 \gamma_G^2},$$

where

$$k_y^2 \simeq \left(\frac{m^0}{r_s} \right)^2,$$

and

$$\sigma_R \simeq \frac{1}{|2\epsilon_v|^{1/2} \Delta_x \delta_G}.$$

Therefore

$$\delta_R \simeq |2\epsilon_v|^{1/4} (\Delta_x \delta_G)^{1/2}$$

In conclusion

$$\gamma \simeq \left(\frac{m^0}{r_s} \rho_s \right)^2 \frac{v_{ei}^{\parallel} m_e}{k_{\parallel}^2 T_e} \gamma_G^2 \left[1 + \frac{\delta_G}{\Delta_x |2\epsilon_v|^{1/2}} \right]$$

or

$$\gamma \simeq \left(\frac{m^0}{r_s} \rho_s \right)^2 \frac{v_{ei}^{\parallel} m_e}{k_{\parallel}^2 T_e} \gamma_G^2 + \left(\frac{v_{ei}^{\parallel} m_e}{2k_{\parallel}^2 T_e} \right)^{1/2} \gamma_G |\omega_{TT}^0| \frac{\rho_s}{\Delta_x} \\ \times \left(1 - \frac{\omega_{di}}{\omega_{TT}} \right)^{1/2}$$

2-D Peaking Mode?

$$\hat{n} \simeq \tilde{n}(r - r_s, \theta) \exp \left\{ -i\omega t + in^0 [\varphi - q(r_s)\theta] - in^0 [q(r) - q(r_s)] F(\theta) \right\}$$

Appendix

Now we give the approximate numerical estimates for a set of parameters that are involved in the theory of the Quasi-Coherent Mode discussed earlier. These estimates are based on the relevant experimental observations [1] made by the Alcator C-Mod machine.

- Frequency Range

$$f \sim 100 \text{ kHz}, \quad \omega \sim 6.3 \times 10^5 \text{ rad} \cdot \text{sec}^{-1}.$$

- Major Radius of the Plasma Column

$$R_0 \simeq 68 \text{ cm}.$$

- Location of the Mode Center R_{mc}

$$R_{mc} \simeq R_{LCFS} \text{ — LCFS stands for the Last Closed Flux Surface.}$$

- Mode Radial Width

$$\Delta r \simeq 3 \text{ mm}.$$

- Sign of E_r inside the mode layer

$$E_r = -\frac{\partial \phi}{\partial r} > 0.$$

Therefore $v_E/v_{di} > 0$.

- Range of Poloidal Mode Phase Velocity $v_{ph} \equiv \omega/k_\theta$

$$v_{*e} < v_{ph} - v_E < v_{de}$$

where the electron temperature gradient is significant across the layer in which the QCM is excited.

- Density Fluctuation Level

$$\frac{\tilde{n}}{n} \sim 30\%.$$

- Electron Temperature Fluctuation Level

$$\frac{\tilde{T}_e}{T_e} \sim 45\%.$$

- Electric Potential Fluctuation Level

$$\frac{e\tilde{\phi}}{T_e} \sim 45\%.$$

- Electron Temperature at R_{LCFS}

$$T_e \simeq 50 \text{ eV.}$$

- Electron Density at $R \simeq R_{LCFS}$

$$n_e \simeq 1.5 \times 10^{20} \text{ m}^{-3}.$$

- Poloidal Wavenumber

$$k_\theta \sim 1.5 \text{ rad/cm.}$$

- Thermal Velocities

$$v_{thi} \simeq 6.9 \times 10^6 \left[\frac{T_i}{50 \text{ eV}} \right]^{\frac{1}{2}} \text{ cm} \cdot \text{sec}^{-1} \quad \text{deuteron}$$

$$v_{the} \simeq 3.0 \times 10^8 \left[\frac{T_e}{50 \text{ eV}} \right]^{\frac{1}{2}} \text{ cm} \cdot \text{sec}^{-1} \quad \text{electron}$$

- Collisional Frequencies

deuterons

$$\nu_{ii} \simeq 1.73 \times 10^5 \left[\frac{n_i}{1.5 \times 10^{14} \text{ cm}^{-3}} \right] \left[\frac{\ln \Lambda}{12} \right] \left[\frac{50 \text{ eV}}{T_i} \right]^{\frac{3}{2}} \text{ sec}^{-1}.$$

electron - deuteron

$$\nu_{ei} \simeq 1.48 \times 10^7 \left[\frac{n_i}{1.5 \times 10^{14} \text{ cm}^{-3}} \right] \left[\frac{\ln \Lambda}{12} \right] \left[\frac{50 \text{ eV}}{T_i} \right]^{\frac{3}{2}} \text{ sec}^{-1}.$$

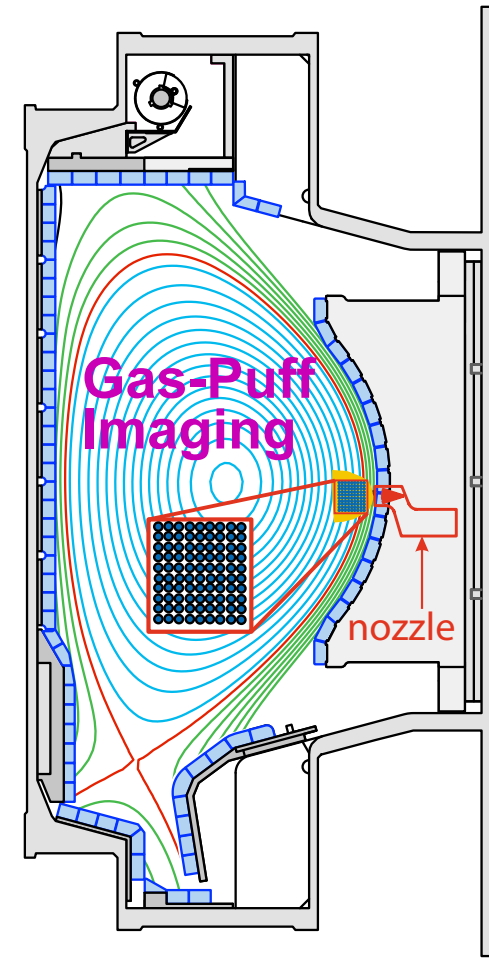
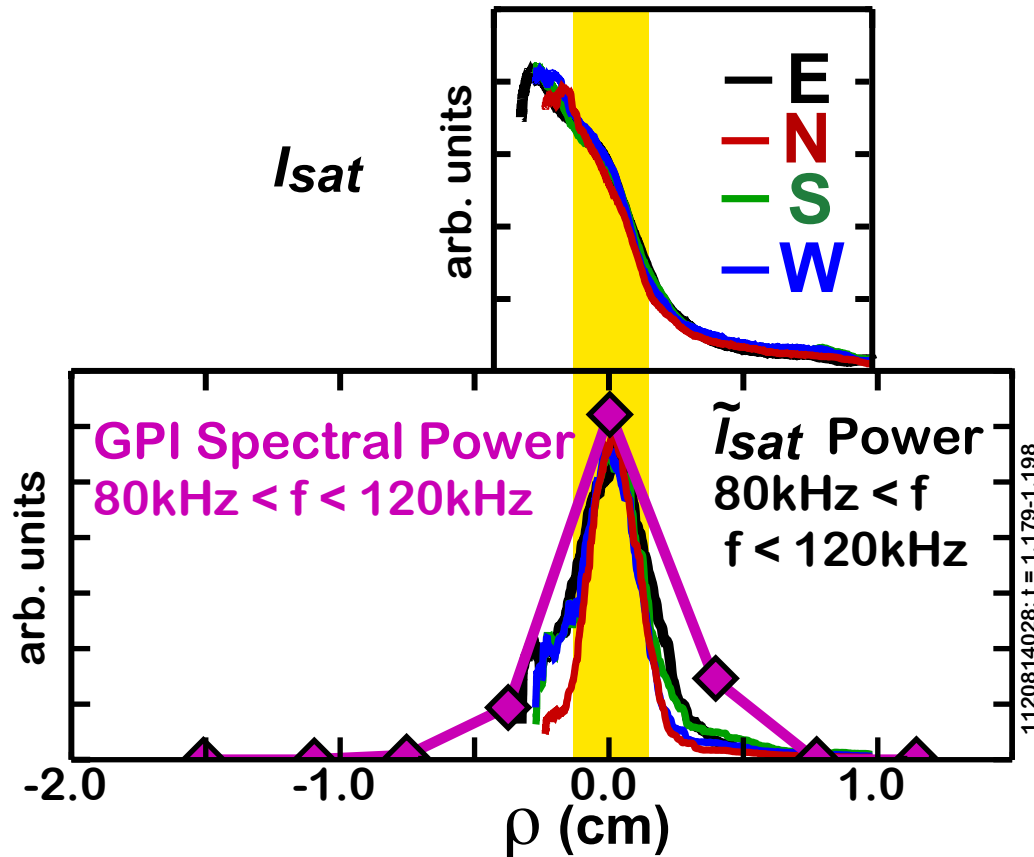
- Mean Free Paths

$$\lambda_{ii} \simeq 4.0 \times 10^1 \left[\frac{v_{thi}}{6.9 \times 10^6 \text{ cm} \cdot \text{sec}^{-1}} \right] \cdot \left[\frac{1.73 \times 10^5 \text{ sec}^{-1}}{\nu_{ii}} \right] \text{ cm.}$$

$$\lambda_{ee} \simeq 2.0 \times 10^1 \left[\frac{v_{the}}{3.0 \times 10^8 \text{ cm} \cdot \text{sec}^{-1}} \right] \cdot \left[\frac{1.48 \times 10^7 \text{ sec}^{-1}}{\nu_{ee}} \right] \text{ cm.}$$

Narrow QCM layer width from ion saturation current fluctuations is consistent with Gas-Puff Imaging (GPI)

I_{sat} , \tilde{I}_{sat} and GPI Fluctuation Profiles

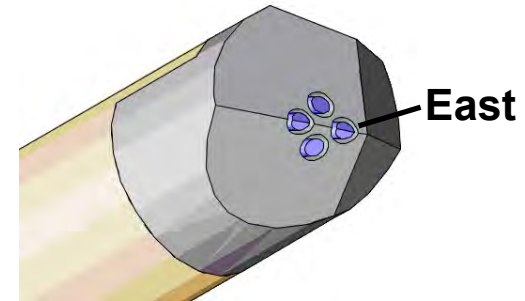
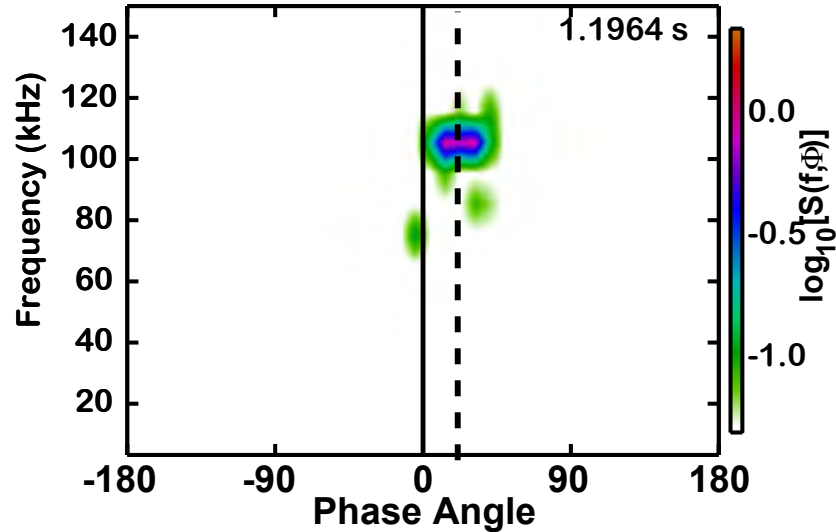


- I_{sat} and \tilde{I}_{sat} power profiles align, despite being recorded at different times by different probes
- Conclusion: QCM is not being attenuated by probe
- Narrow QCM layer is consistent with Gas-Puff Imaging (allowing shift)

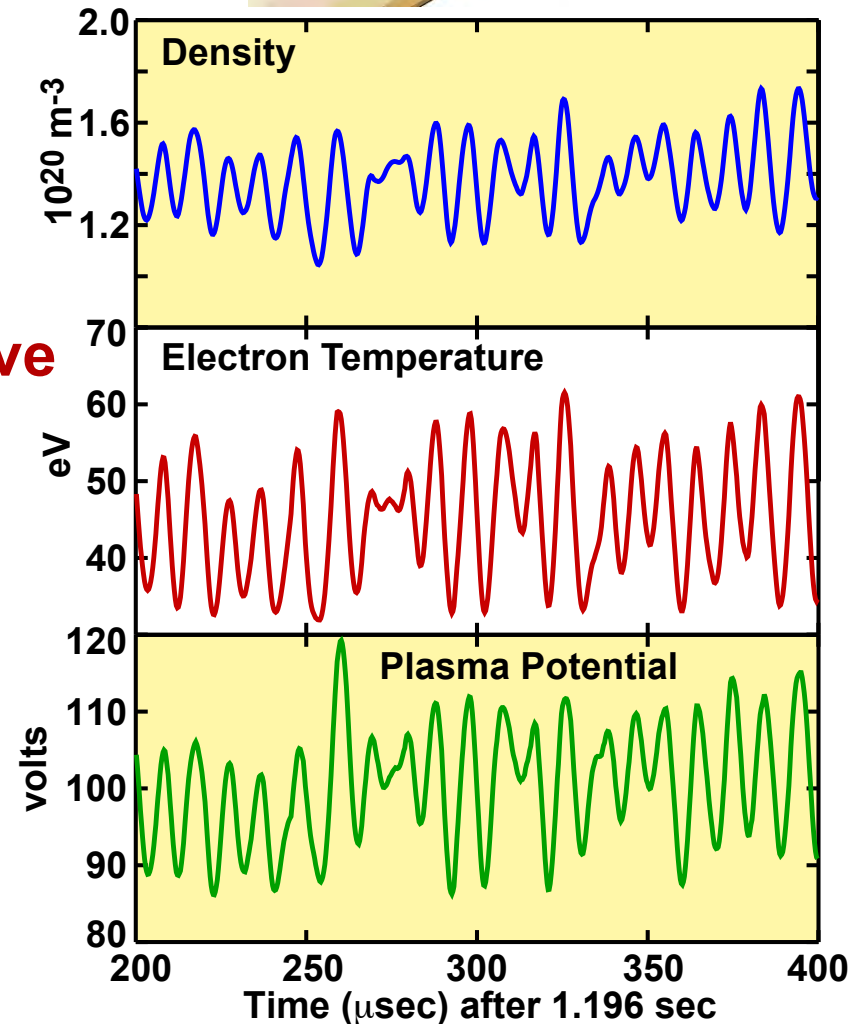
● Radial width of Quasi-Coherent Mode layer is ~ 3 mm FWHM

Snapshot of QCM reveals large amplitude, ~in-phase, density, electron temperature and potential fluctuations

Cross Power Spectrum: **Density** and **Potential**

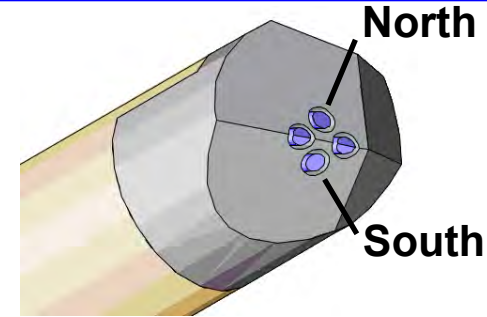
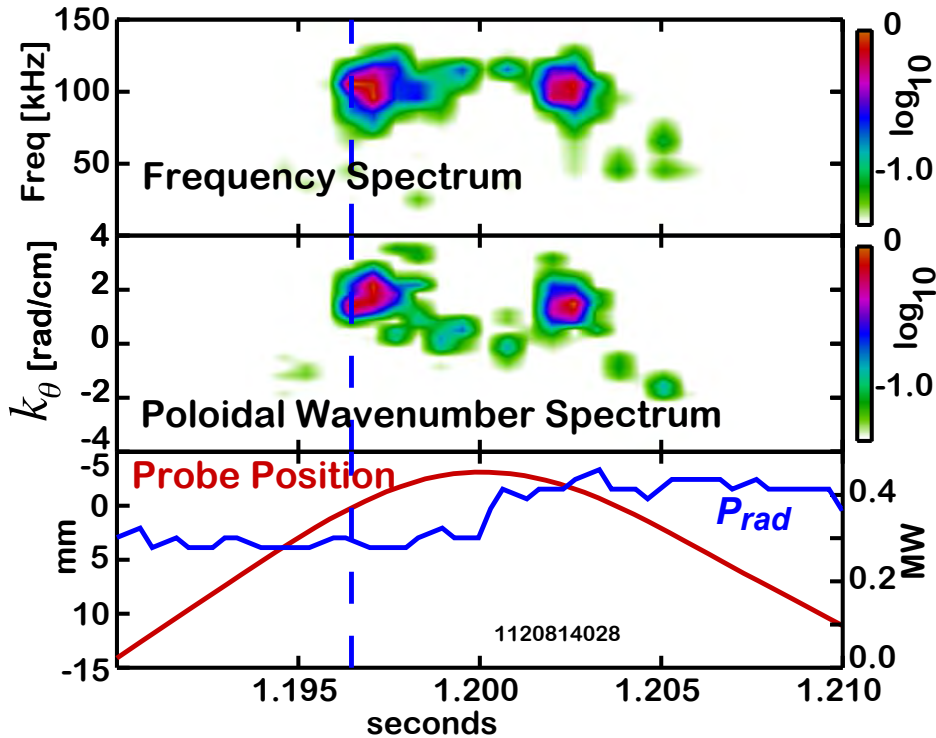


Potential lags **Density** with a phase angle of ~ 16 degrees => **Drift wave**

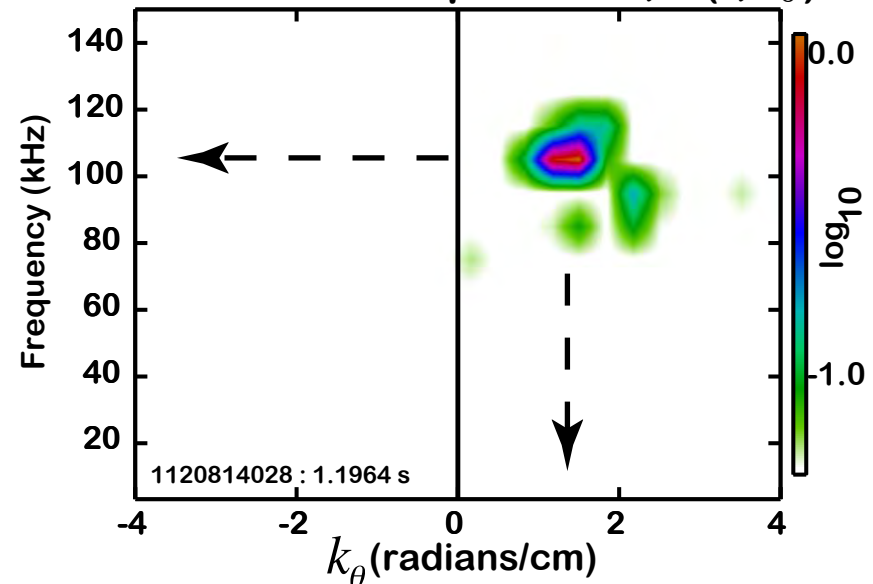


MLP passes through mode layer -- reveals density fluctuation with frequency and wavenumber of QCM

Spectra from North-South electrodes



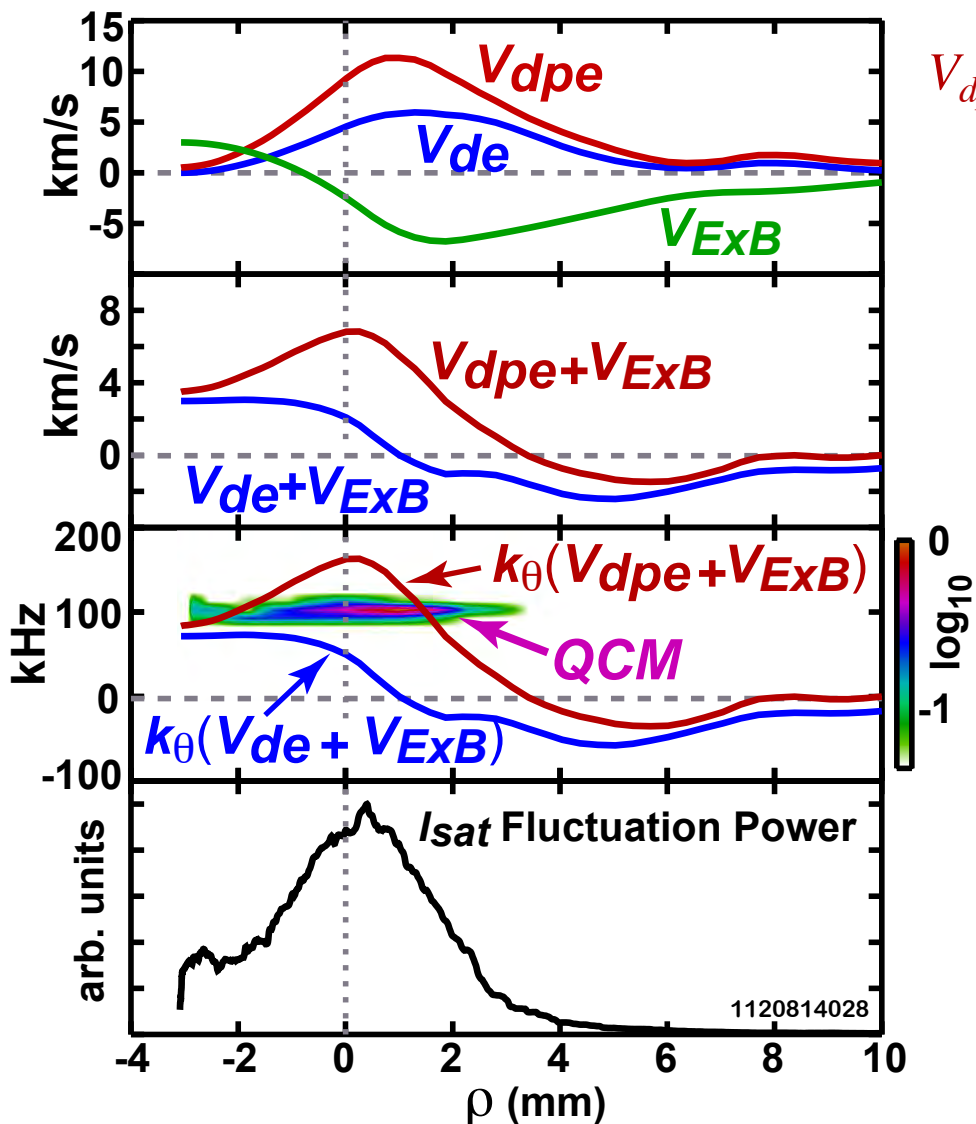
Cross-Power Spectrum, $S(f, k_\theta)$



- Mode exists near LCFS
- Frequency, poloidal wave number and propagation in electron diamagnetic direction -- consistent with B_θ probe, PCI (and GPI)
- Probe appears to pass through mode
- Probe perturbs plasma at peak insertion (see P_{rad} jump)
Post mortem: leading edge of probe head showed melt damage
- Must examine other electrodes to see if probe is perturbing mode...

Quasi-coherent mode propagates at electron diamagnetic drift velocity in the plasma frame

Velocities computed from East electrode profiles

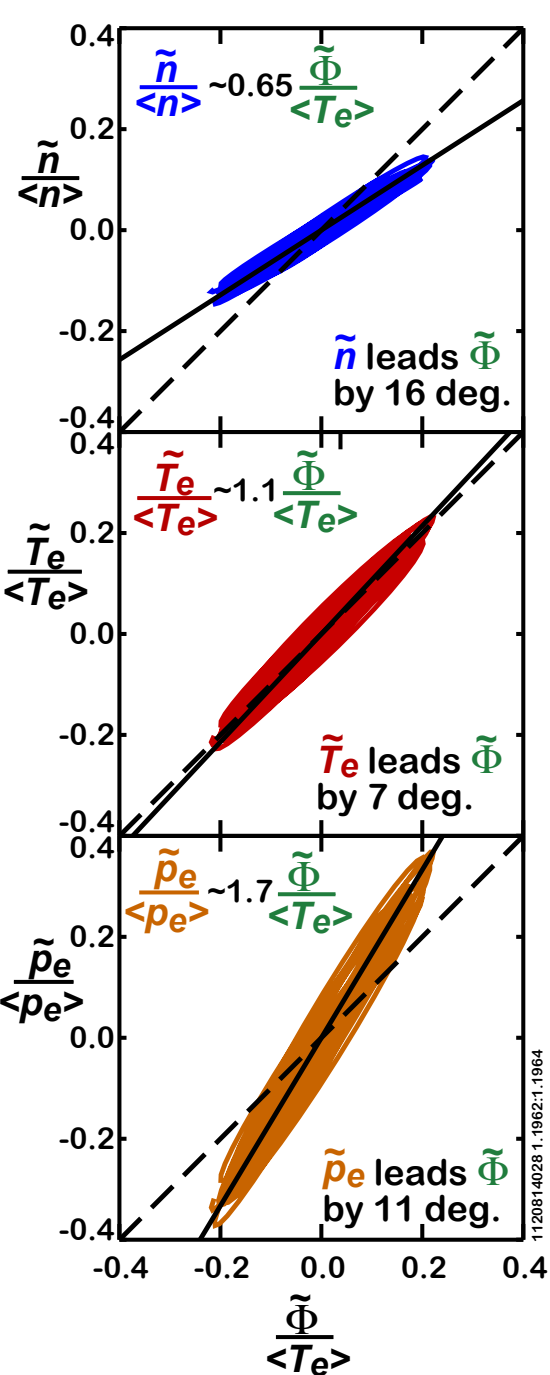


$$V_{dpe} = \frac{\nabla_r n T_e \times \underline{b}}{nB} \quad V_{de} = \frac{T_e \nabla_r n \times \underline{b}}{nB} \quad V_{ExB} = \frac{\underline{b} \times \nabla_r \Phi}{B}$$

- V_{dpe} , V_{de} are in opposite directions to V_{ExB} in mode layer
- V_{dpe} , V_{de} are stronger than V_{ExB} in mode layer
- QCM propagates in e^- dia. direction in the plasma frame

QCM frequency is quantitatively consistent with $k_\theta \sim 1.5$ rad/cm mode propagating with velocity between V_{dpe} and V_{de} in the plasma frame.

Analysis of \tilde{n} , $\tilde{\Phi}$, \tilde{T}_e , \tilde{p}_e indicates interchange drive and inductive $\tilde{E}_{//}$ components contribute to QCM



- Phase order is $\tilde{n}(0^\circ)$, $\tilde{p}_e(5^\circ)$, $\tilde{T}_e(9^\circ)$, $\tilde{\Phi}(16^\circ)$
=> drift wave

- Large electron pressure fluctuation

$$\frac{\tilde{p}_e}{\langle p_e \rangle} \sim 1.7 \frac{\tilde{\Phi}}{\langle T_e \rangle}$$



Massachusetts Institute of
Technology



Columbus
Superconductors SpA



Laboratoire National des
Champs Magnétiques Intenses

Cooperation on the development of MgB₂ towards the realization of high field hybrid magnets

Grenoble (France), 22 September 2010

Building upon the distinctive as well as highly complementary know-how on the development and characterization of superconducting materials and magnets, and their potential implementation in Plasma Physics experiments, the undersigned agree to cooperate closely, together with their collaborators:

- For the performance evaluation of improved MgB₂ wires
- For the study of MgB₂-based superconducting magnets capable of producing fields in excess of 10 Tesla over a large bore
- For the study of energy-efficient hybrid magnet solutions based on MgB₂
- For the study of the application of such magnets in various branches of Physics including Plasma Physics
- In the effort to secure funding at the international level in order to facilitate the accomplishment of these actions

Prof. B. Coppi
Head, High Energy Plasmas

International Undertaking, M.I.T.

Dr. G. Grasso
General Director

Columbus Superconductors SpA

Dr. G. Rikken

Director

LNCMI, Grenoble (France)

From: "Eugenio Nappi" <Eugenio.Nappi@ba.infn.it>
Subject: Incontro in presidenza INFN
Date: Thu, June 19, 2014 7:27 am
To: coppi@psfc.mit.edu
Cc: "Attilio Ferrari" <ferrari87@gmail.com>, "Eugenio Nappi" <Eugenio.Nappi@ba.infn.it>

Gent.mo prof. Coppi,
ho saputo dal prof. Ferrari che la prossima settimana Ella si troverà in Italia.

La contatto per chiedere la Sua disponibilità ad un incontro in presidenza INFN, a Roma, nel pomeriggio di lunedì 23, quando desidera tra le 15 e le 20, o di martedì 24, tra le 15 e le 16. Immagino si ricorda che ci siamo già incontrati un paio di anni fa con i proff. Masiero e Fortuna, sempre in presidenza INFN, appena ricevemmo il mandato dal MIUR di collaborare con Lei sul progetto IGNITOR.

Come sa, il prof. Ferroni mi ha chiesto di coordinare le attività del costituendo team italiano che, coadiuvato da un team russo, ha il compito di elaborare la documentazione necessaria alla successiva realizzazione del progetto.

La ringrazio per l'attenzione che vorrà dedicare al mio invito. Con l'auspicio

di poterLa incontrare al più presto, La saluto cordialmente.

Eugenio Nappi

(componente della Giunta Esecutiva dell'INFN)
